First-, third-, and fifth-order resonant spectroscopy of an anharmonic displaced oscillators system in the condensed phase

Yoshitaka Tanimura and Ko Okumura
Institute for Molecular Science, Myodaiji, Okazaki 444, Japan

(Received 3 September 1996; accepted 22 October 1996)

We have obtained *N*th-order response functions for a two-level system described by displaced anharmonic potential surfaces coupled to a heat bath. The anharmonicity of the potentials has been taken into account as a perturbation of harmonic potentials. The heat-bath was assumed to be an ensemble of harmonic oscillators. Coupling between the two-level system and the bath was assumed to be bilinear. The calculations were done analytically using the Liouville-space generating functional, which had been obtained by way of the path-integral approach. The response functions have been defined in terms of line-shape functions with these line-shape functions being expressed in terms of the bath spectral density and the temperature. We have carried out model calculations of the first-, third-, and fifth-order optical processes for various parameters of anharmonicity to show that anharmonicity plays a minor role in linear absorption, impulsive pump–probe, and photon echo experiments, but plays a major role, in some cases, in fifth-order two-dimensional resonant spectroscopy which is proposed in this paper. © *1997 American Institute of Physics.*
[S0021-9606(97)50405-3]

I. INTRODUCTION

In addition to information about essentially static structure, vibrational line shapes in the condensed phase contain information from a variety of dynamic processes, including such important processes as microscopic dynamics, intermolecular couplings, and time scales of solvent evolution that modulate the energy of a transition. Each of these processes involves coupling between the internal vibrations of a molecule and the external degrees of freedom of its environment. However, since vibrational lines from these processes are often broadened and also appear in similar positions, it is not easy to distinguish them from linear spectroscopy.

This difficulty can be overcome by higher-order (nonlinear) optical processes involving many laser interactions. The simplest and most common such techniques are four-wave mixing related to third-order nonlinearity. There are numerous spectroscopic techniques related to this order including pump–probe spectroscopy,[1,2] photon echo,[3,4] hole burning,[5,6] and coherent anti-Stokes Raman.[7,8] These techniques make it possible to utilize more than one time-evolution period and allow us to distinguish dynamical processes in which their time responses are different.[9]

Recent advances in femtosecond laser technology has allowed us to perform even higher-order spectroscopy. Raman echo experiments proposed by Loring and Mukamel are related to seventh-order nonlinearity and can selectively probe the homogeneous linewidth.[10] Several experiments and theoretical studies, including related IR echo experiments, have been subsequently carried out in order to measure the homogeneous vibrational linewidth.[11–15] These experiments were conducted on isolated intramolecular high frequency vibrations and they employed laser pulses longer than the vibrational periods. Two-dimensional off-resonant spectroscopy (2DOS) proposed by Tanimura and Mukamel[16] has been designed to separate the inhomogeneous distribution of slowly varying parameters, for example of local liquid configurations, from the total spectral distribution of the dynamical time scale. This 2DOS experiment uses two pairs of excitation pulses and is related to fifth-order nonlinearity. Several experimental and theoretical studies have been carried out to explore the possibility of detecting such inhomogeneity.[17–20] 2DOS can also be applied to study phonon dynamics in solid[21] and anharmonicity of vibrational modes.[22] Raman echo and 2DOS experiments were based on off-resonance laser excitation techniques, which neglect dynamics on excitation states. Cho and Fleming suggested a new fifth-order spectroscopy using three electronically-resonant pulses[23] and this experiment has subsequently been carried out.[24] This fifth-order, three pulses scattering (FOTS) differs from 2DOS, since FOTS separates the homogeneous contribution of a vibrational spectrum from the inhomogeneity of an electronic transition energy, whereas 2DOS separates the inhomogeneity of the vibrational modes themselves.

It is obvious that higher-order spectroscopy can contain many time intervals and these can be used to separate the targeting dynamical processes from the others such as the inhomogeneity of the vibration modes; however, analysis of such signals becomes much more complex compared with that of lower-order ones. Since one needs to deal with various time configurations of lasers pulses in higher order optical processes as a function of various physical parameters, compact theoretical expressions are essential to interpret the experimental studies. In this paper, we present *N*th-order response functions for a displaced anharmonic oscillators system coupled to a heat bath and explore the possibilities of using higher-order optical processes to study the anharmonicity of potentials.

The theoretical calculation of higher-order optical processes of anharmonic potential systems poses some difficult problems. Optical processes can be calculated using a direct

 0021-9606/97/106(6)/2078/18/$10.00

integration of the equations of motion in the presence of a laser field. By calculating the relevant density matrix elements, it is possible to study optical processes of arbitrary order. Dephasing processes induced by a heat bath can be incorporated using equations of motion for a reduced density matrix, such as the quantum master equation[25] or the quantum Fokker–Planck equation for multipotential surfaces.[26] These equations of motion have capability of dealing with anharmonic potential surfaces, however, solving such equations of motion for various physical conditions is computationally very intensive. In addition, the Nth order time-correlation functions have to be calculated to obtain the $(N-1)$th order optical processes, and this is very difficult to calculate using the equations of motion approach. Thus, higher-order optical processes, using equation of motion approach, have not been successfully studied.

Alternatively, optical processes can be calculated using the response function approach, which is based on a perturbative expansion of the optical polarization in powers of a laser field.[27] This approach has been successfully applied to the study of lower order optical processes such as four-wave mixing experiments.[9] If one limits oneself to the study of a two-level system represented by displaced harmonic potentials, exact closed expressions for an Nth order response function can be obtained using path-integral techniques.[28,29] In addition, it is possible to include any coordinate dependence of transition dipole moments on coordinates (non-Condon effects) to an Nth order response function.[30] These studies have so far been limited to the harmonic oscillators system. But, recently, we have developed a nonequilibrium generating functional theory, which includes the anharmonicity of the potential in the Brownian oscillator model.[31] We then studied the effects of anharmonicity on the third-, fifth-, and higher-order off-resonant spectroscopy.[3] In the present paper, we generalize previous results of generating functions for a single potential surface, to multipotential ones, and calculate the first-, third-, and fifth-order response functions in order to study the effects of anharmonicity on resonant spectroscopy.

The organization of the paper is as follows: In Sec. II we present the Liouville-space generating functions by extending the generating functional obtained in Ref. 31. In Sec. III, we define the anharmonic potential system and present the Nth order response functions. In Sec. IV we write down the first-, third-, and fifth-order polarizations and response functions for an anharmonic displaced oscillators system. In Sec. V, the linear absorption, pump–probe and photon-echo spectroscopies are studied numerically for various anharmonic parameters. In Sec. VI, we propose two-dimensional resonance spectroscopy and show its ability to distinguish the effects of anharmonicity from the others. Section VII is devoted to concluding remarks.

II. NONEQUILIBRIUM GENERATING FUNCTIONALS FOR LIOUVILLE-SPACE PATHS

Consider a model Hamiltonian commonly used in the description of such phenomena as elementary excitations,[32,33] nonlinear optical response,[34–36] nonadiabatic transitions,[37,29,38,39] and tunneling.[40,41] The primary quantum system is taken to be a two level system with a ground state $|g\rangle$ and an excited state $|e\rangle$, and its Hamiltonian is given by (see Fig. 1)

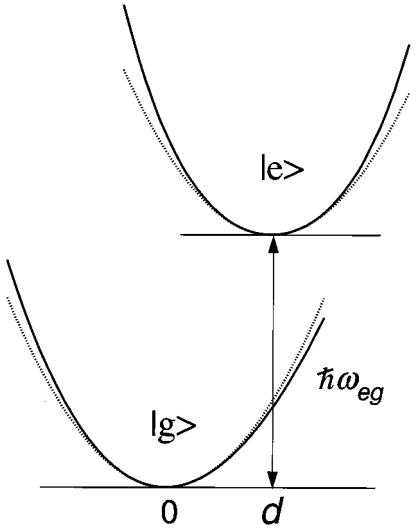

FIG. 1. Potential surfaces of the anharmonic displaced oscillators system. The lower state is denoted by $|g\rangle$, the upper by $|e\rangle$. The equilibrium coordinate displacement and the energy difference between the two potentials are expressed by d and $\hbar\omega_{eg}$, respectively. The dotted lines represent the unperturbed harmonic potential surfaces. Here, we considered a cubic perturbation ($\propto -q^3$) to the ground state and a quadratic one ($\propto q^4$) to the excited state.

$$H_S = H_0 + E(t)H_I, \tag{2.1}$$

where

$$H_0 = |g\rangle H_g \langle g| + |e\rangle H_e \langle e|, \tag{2.2}$$

with

$$H_g = \frac{p^2}{2M} + U_g(q), \quad H_e = \frac{p^2}{2M} + U_e(q), \tag{2.3}$$

and p, q, and M represent the momentum, the coordinate, and the mass, respectively. The interaction consists of the time dependent function, $E(t)$, and the operator, H_I, which is given by

$$H_I = \mu(|g\rangle\langle e| + |e\rangle\langle g|). \tag{2.4}$$

In optical problems, $E(t)$ and μ represent the radiation field and the dipole interaction between the two states, respectively. In nonadiabatic curve crossing problems, $E(t)=1$ and μ represent the nonadiabatic interaction between the two states $|e\rangle$ and $|g\rangle$.

Let us assume that the system is coupled to an environment consisting of a set of harmonic oscillators with coordinates x_n and momenta p_n. The interaction between the system and the nth oscillator is assumed to be linear with a coupling strength c_n. The total Hamiltonian is then given by

$$H = H_S + H', \tag{2.5}$$

where

$$H'=\sum_n \left[\frac{p_n^2}{2m_n}+\frac{m_n\omega_n^2}{2}\left(x_n-\frac{c_n q}{m_n\omega_n^2}\right)^2\right]. \tag{2.6}$$

We have followed the common notation of Grabert, Schramm, and Ingold.[42] The character of the heat-bath is specified by the spectral distribution

$$J(\omega)=\pi\sum_n \frac{c_n^2}{2m_n\omega_n}\delta(\omega-\omega_n). \tag{2.7}$$

The total system is assumed to be initially at equilibrium in the ground electronic state

$$\rho_g=|g\rangle\langle g|\exp[-\beta(H_g+H')]/\mathrm{Tr}\{\exp[-\beta(H_g+H')]\}, \tag{2.8}$$

where $\beta\equiv 1/k_BT$ is the inverse temperature. Since we are not interested in the dynamics of the environment, we trace over its coordinates. We thus introduce the reduced density matrix

$$\rho(t)\equiv \mathrm{Tr}_B\{\rho_{\mathrm{tot}}(t)\}. \tag{2.9}$$

Here, $\mathrm{Tr}_B\{\ \}$ represents the trace over the environment (the bath) degrees of freedom and $\rho_{\mathrm{tot}}(t)$ is the total (system + bath) density matrix. By expanding the density matrix of the system $\rho(t)$, in terms of the interaction H_I, we have

$$\rho(t)=\sum_{N=0}^{\infty}\int_0^t d\tau_N\int_0^{\tau_N}d\tau_{N-1}\cdots\int_0^{\tau_2}d\tau_1 E(\tau_N)E(\tau_{N-1})\times\cdots E(\tau_1)\rho^{(N)}(t,\tau_N,\tau_{N-1},\ldots,\tau_1), \tag{2.10}$$

where

$$\begin{aligned}\rho^{(N)}(t,\tau_N,\tau_{N-1},\ldots,\tau_1)&=\left(-\frac{i}{\hbar}\right)^N\mathrm{Tr}_B\left\{\exp\left[-\frac{i}{\hbar}(t-\tau_N)(H_0+H')^{\times}\right]H_I^{\times}\right.\\&\times\exp\left[-\frac{i}{\hbar}(\tau_N-\tau_{N-1})(H_0+H')^{\times}\right]\\&\left.\times H_I^{\times}\cdots H_I^{\times}\exp\left[-\frac{1}{\hbar}(\tau_2-\tau_1)(H_0+H')^{\times}\right]H_I^{\times}\rho_g\right\}.\end{aligned} \tag{2.11}$$

In the above we used the superoperator notation $\times$ defined by

$$A^{\times}B\equiv AB-BA,\quad A^{\times}B^{\times}C\equiv A(BC-CB)-(BC-CB)A,\qquad \exp[A^{\times}]B\equiv\exp[A]B\exp[-A], \tag{2.12}$$

and so forth, where A, B, and C are operators. Since each $H_I^{\times}$ can act either from the left or from the right, and since $\rho^{(n)}$ contains $nH_I^{\times}$ factors, Eq. (2.11) naturally separates into $M=2^N$ terms denoted *Liouville-space paths*.[9] In practice we need to evaluate only half of these terms, since they always come in Hermitian conjugate pairs, and $\rho^{(n)}$ are Hermitian. We thus have

$$\rho^{(N)}(t,\tau_N,\tau_{N-1},\ldots,\tau_1)=\sum_{\alpha=1}^{M/2}\rho_{\alpha}^{(N)}(t)+\mathrm{h.c.}, \tag{2.13}$$

where α labels the paths. The function $\rho_{\alpha}^{(N)}(t)$ represents the contributions of the αth Liouville-space path to the density matrix evaluated to Nth order in H_I, and will be devoted to the Liouville-space generating functions (LGF). Note that the LGF, $\rho^{(N)}(t)$, depends on all time variables τ_N and not just on t. The τ_n dependence is incorporated in the α subscript since each path α represents a specific choice of time arguments. For $N=2$, for example, there are two possible Liouville-space paths plus their Hermitian conjugates. These are defined as (corresponding double-sided Feynman diagrams are given in Ref. 30)

$$\begin{aligned}\rho_1^{(2)}(t)\equiv\mathrm{Tr}_B\left\{\exp\left[-\frac{i}{\hbar}\int_{\tau_2}^t dt(H_g+H')\right]\mu\right.&\times\exp\left[-\frac{i}{\hbar}\int_{\tau_1}^{\tau_2}dt(H_e+H')\right]\mu\\&\times\exp\left[-\frac{i}{\hbar}\int_0^{\tau_1}dt(H_g+H')\right]\rho_g\\&\left.\times\exp\left[\frac{i}{\hbar}\int_0^t dt(H_g+H')\right]\right\}\end{aligned} \tag{2.14}$$

and

$$\begin{aligned}\rho_2^{(2)}(t)=\mathrm{Tr}_B\left\{\exp\left[-\frac{i}{\hbar}\int_{\tau_1}^t dt(H_e+H')\right]\mu\right.&\times\exp\left[-\frac{i}{\hbar}\int_0^{\tau_1}dt(H_g+H')\right]\\&\times\rho_g\exp\left[\frac{i}{\hbar}\int_0^{\tau_2}dt(H_g+H')\right]\mu\\&\left.\times\exp\left[\frac{i}{\hbar}\int_{\tau_2}^t dt(H_e+H')\right]\right\}.\end{aligned} \tag{2.15}$$

Each of the Liouville-space paths can be expressed as

$$\rho_{\alpha}^{(N)}(t)=\mathrm{Tr}_B\left(\exp\left\{-\frac{i}{\hbar}\int_0^t dt[H_L(t)+H']\right\}\times\rho_g\exp\left\{\frac{i}{\hbar}\int_0^t dt[H_R(t)+H']\right\}\right), \tag{2.16}$$

where

$$H_L(t)=\frac{p^2}{2M}+U_L(q;t),\quad H_R(t)=\frac{p^2}{2M}+U_R(q;t), \tag{2.17}$$

and U_L and U_R are the potentials of the left-hand side (ket) and the right-hand side (bra), respectively, of the density matrix, and we set $\mu=1$. The various Liouville-space paths, denoted by α, simply differ by the specific choices of U_L and U_R. As an example, the potentials for the paths corresponding to Eqs. (2.14) and (2.15) are given in Table I. By introducing these potentials, we can derive a single formal expression, which will hold for all paths.

In the path integral formalism, the time propagators and the initial density matrix can be expressed in the functional of the coordinates $q(t)$ and $x(t)$ as

TABLE I. Potentials of the left (ket) and right (bra) hand side of the density matrix corresponding to the Liouville-space paths for Eqs. (2.14) and (2.15).

α	$U(q,s)$	$0\sim\tau_1$	$\tau_1\sim\tau_2$	$\tau_2\sim t$
1	$U_L(q,s)$	$U_g(q)$	$U_e(q)$	$U_g(q)$
	$U_R(q',s)$	$U_g(q')$	$U_g(q')$	$U_g(q')$
2	$U_L(q,s)$	$U_g(q)$	$U_e(q)$	$U_e(q)$
	$U_R(q',s)$	$U_g(q')$	$U_g(q')$	$U_e(q')$

$$\langle q,x|\exp\left\{-\frac{i}{\hbar}\int_0^t dt[H_L(t)+H']\right\}|q_i,x_i\rangle = \int_{q(0)=q_i}^{q(t)=q} D[q(t)]\int_{x(0)=x_i}^{x(t)=x} D[x(t)]\exp\left\{\frac{i}{\hbar}S_L[q,x;t,0]\right\}, \tag{2.18}$$

$$\langle q_i',x_i'|\exp\left\{\frac{i}{\hbar}\int_0^t dt[H_R(t)+H']\right\}|q',x'\rangle = \int_{q'(0)=q_i'}^{q'(t)=q'} D[q'(t)]\int_{x'(0)=x_i'}^{x'(t)=x'} D[x'(t)] \times\exp\left\{-\frac{i}{\hbar}S_R[q',x';t,0]\right\}, \tag{2.19}$$

and

$$\langle q_i,x_i|\rho_g|q_i',x_i'\rangle \equiv \int_{\overline{q}(0)=q_i}^{\overline{q}(\beta\hbar)=q_i'} D[\overline{q}(\tau)]\int_{\overline{x}(0)=x_i}^{\overline{x}(\beta\hbar)=x_i'} D[\overline{x}(\tau)] \times\exp\left\{-\frac{1}{\hbar}S_\beta[\overline{q,x;\tau},0]\right\}, \tag{2.20}$$

where the actions S_L, S_R, and S_β are defined by

$$S_L[q,x;t,0]=\frac{1}{2}\int_0^t ds\left\{M\left(\frac{dq}{d\tau}\right)^2-2U_L(q;t) +\sum_{j=1}^{\infty}\left[m_j\left(\frac{dx_j}{d\tau}\right)^2-m_j\omega_j^2\left(x_j-\frac{c_jq}{m_j\omega_j^2}\right)^2\right]\right\}, \tag{2.21}$$

$$S_R[q',x';t,0]=\frac{1}{2}\int_0^t ds\left\{M\left(\frac{dq'}{d\tau}\right)^2-2U_R(q';t) +\sum_{j=1}^{\infty}\left[m_j\left(\frac{dx_j'}{d\tau}\right)^2-m_j\omega_j^2\left(x_j'-\frac{c_jq'}{m_j\omega_j^2}\right)^2\right]\right\}, \tag{2.22}$$

and

$$S_\beta[\overline{q,x;\beta\hbar},0]=\frac{1}{2}\int_0^{\beta\hbar} ds\left\{M\left(\frac{d\overline{q}}{d\tau}\right)^2+2U_g(\overline{q;\tau}) +\sum_{j=1}^{\infty}\left[m_j\left(\frac{d\overline{x_j}}{d\tau}\right)^2+m_j\omega_j^2\left(\overline{x_j}-\frac{c_j\overline{q}}{m_j\omega_j^2}\right)^2\right]\right\}. \tag{2.23}$$

Thus, by inserting the completeness relations, $|q_i,x_i\rangle\int dq_i\int dx_i\langle q_i,x_i|$ and $|q_i',x_i'\rangle\int dq_i'\int dx_i'\langle q_i',x_i'|$, the reduced density matrix Eq. (2.16) is rewritten in the path integral form as

$$\begin{aligned}\langle q|\rho_\alpha^{(N)}(t)|q'\rangle\equiv\rho_\alpha(q,q',t) &= \int dq_i\int dq_i'\int_{q(0)=q_i}^{q(t)=q} D[q(t)]\int_{q'(0)=q_i'}^{q'(t)=q'} D[q'(t)]\int_{\overline{q}(0)=q_i}^{\overline{q}(\beta\hbar)=q_i'} D[\overline{q}(\tau)]\int dx\int dx'\,\delta(x-x')\\ &\times\int dx_i\int dx_i'\int_{x(0)=x_i}^{x(t)=x} D[x(t)]\int_{x'(0)=x_i'}^{x'(t)=x'} D[x'(t)]\int_{\overline{x}(0)=x_i}^{\overline{x}(\beta\hbar)=x_i'} D[\overline{x}(\tau)]\\ &\times\exp\left\{\frac{i}{\hbar}S_L[q,x;t,0]\right\}\exp\left\{-\frac{1}{\hbar}S_\beta[\overline{q,x;\tau},0]\right\}\exp\left\{-\frac{i}{\hbar}S_R[q',x';t,0]\right\},\end{aligned} \tag{2.24}$$

where the trace operator $\mathrm{Tr}_B\{\}$ is expressed as $\int\int dxdx'\,\delta(x-x')$.

We now specify the ground- and excited-state potentials. The potentials in Eq. (2.3) are represented by

$$U_g(q)=U_g^0(q)+V_g(q),\quad U_e(q)=U_e^0(q)+V_e(q), \tag{2.25}$$

where the harmonic parts are expressed as

$$U_g^0(q)\equiv\frac{M\omega_0^2}{2}q^2,\quad U_e^0(q)\equiv\hbar\omega_{eg}^0+\frac{M\omega_0^2}{2}(q-D)^2. \tag{2.26}$$

The anharmonic parts are expressed as the polynomial function of q and their explicit forms will be given in the next section. We treat the anharmonic part of the potential as the perturbation. Then, by expanding the anharmonic part up to the first order, the density matrix element can be expressed as

$$\rho_\alpha(q,q',t)=\int dq_i\int dq_i'\int_{q(0)=q_i}^{q(t)=q}D[q(t)]\int_{q'(0)=q_i'}^{q'(t)=q'}D[q'(t)]\int_{\overline{q}(0)=q_i}^{\overline{q}(\beta\hbar)=q_i'}D[\overline{q}(\tau)]\int dx\int dx'\,\delta(x-x')\int dx_i\int dx_i'$$
$$\times\int_{x(0)=x_i}^{x(t)=x}D[x(t)]\int_{x'(0)=x_i'}^{x'(t)=x'}D[x'(t)]\int_{\overline{x}(0)=x_i}^{\overline{x}(\beta\hbar)=x_i'}D[\overline{x}(\tau)]\left\{1-\frac{i}{\hbar}\int_0^t dt''[V_L(q;t'')-V_R(q';t'')]-\frac{i}{\hbar}\int_0^{\beta\hbar}d\tau V_g(\overline{q})\right\}$$
$$\times\exp\left[\frac{i}{\hbar}S_L^0(q,x;t,0)\right]\exp\left[-\frac{1}{\hbar}S_\beta^0(\overline{q,x;}\beta\hbar,0)\right]\exp\left[-\frac{i}{\hbar}S_R^0(q',x';t,0)\right],\tag{2.27}$$

where V_L and V_R are the perturbation part of U_L and U_R, respectively and S_L^0,S_R^0 and S_β^0 are the actions for the harmonic part of the potentials. The initial equilibrium state of the system with anharmonic potential is described in terms of the perturbation, $\int_0^{\beta\hbar}d\tau V_g(\overline{q})/\hbar$.

We can evaluate the above path integral for each Liouville-path, denoted by α, by using the Liouville-space generating functional.[30,31] Here, we consider three-source generating functional,

$$\rho_\alpha(q,q',t;\mathbf{J})=\int dq_i\int dq_i'\int_{q(0)=q_i}^{q(t)=q}D[q(t)]\int_{q'(0)=q_i'}^{q'(t)=q'}D[q'(t)]\int_{\overline{q}(0)=q_i}^{\overline{q}(\beta\hbar)=q_i'}D[\overline{q}(\tau)]\int dx\int dx'\,\delta(x-x')$$
$$\times\int dx_i\int dx_i'\int_{x(0)=x_i}^{x(t)=x}D[x(t)]\int_{x'(0)=x_i'}^{x'(t)=x'}D[x'(t)]\int_{\overline{x}(0)=x_i}^{\overline{x}(\beta\hbar)=x_i'}D[\overline{x}(\tau)]$$
$$\times\exp\left\{\frac{i}{\hbar}S_g^0(q,x;t,0)+\frac{i}{\hbar}\int_0^t dt[J_0(t)+J_1(t)q(t)]\right\}\exp\left\{-\frac{1}{\hbar}S_g^0(\overline{q,x;}\beta\hbar,0)+\frac{1}{\hbar}\int_0^{\beta\hbar}d\tau[J_3(\tau)\overline{q}(\tau)]\right\}$$
$$\times\exp\left\{-\frac{i}{\hbar}S_g^0(q',x';t,0)-\frac{i}{\hbar}\int_0^t dt[J_0'(t)+J_2(t)q'(t)]\right\},\tag{2.28}$$

where S_g^0 is the action for the system potential $U_s^0(q)$ and $\mathbf{J}\equiv\{J_1,J_2,J_3\}$. Note that $J_i(t)$ are the independent functions of the coordinates. We have also added the phase functions $J_0(t)$ and $J_0'(t)$ to take into account the Liouville path. Using the simple identity, $f(\partial/\partial J)e^{Jq}=f(q)e^{Jq}$, the density functional elements in Eq. (2.28) can be calculated from the generating functional by replacing

$$q(t)\to\frac{\hbar}{i}\frac{\partial}{\partial J_1(t)},\quad q'(t)\to\frac{\hbar}{i}\frac{\partial}{\partial J_2(t)},\quad \overline{q(t)}\to\hbar\frac{\partial}{\partial J_3(t)},\tag{2.29}$$

as

$$\rho_\alpha(q,q',t)=\rho_\alpha(q,q',t,\mathbf{J})|_{J=0}$$
$$-\left(\frac{i}{\hbar}\int_0^t dt'\left\{V_L\left[\frac{\hbar}{i}\frac{\partial}{\partial J_1(t')};t\right]\right.\right.$$
$$\left.\left.-V_R\left[\frac{\hbar}{i}\frac{\partial}{\partial J_2(t')};t\right]\right\}+\frac{1}{\hbar}\int_0^{\beta\hbar}d\tau V_g\left[\hbar\frac{\partial}{\partial J_3(\tau)}\right]\right)$$
$$\times\rho_\alpha(q,q',t;\mathbf{J})|_{J=0}.\tag{2.30}$$

Note that the Liouville path α was taken into account by a choice of $J_0(t)$ and $J_0'(t)$ as we will show below.

The potential $U_g^0(q)$ is harmonic and three external forces $J_1(t)q_1(t)$, $J_2(t)q_2(t)$, and $J_3(t)\overline{q(t)}$ are the linear functions of coordinates, we can carry out the functional integral in Eq. (2.28) by obtaining minimal action path[42,30] or by using the Feynman rules.[31] We introduce the center and difference coordinates

$$r\equiv\frac{q+q'}{2},\quad x\equiv q-q',\tag{2.31}$$

respectively. The initial coordinates x_i and r_i are defined accordingly. Similarly we introduce

$$J^{(+)}=\frac{(J_1+J_2)}{2},\quad J^{(-)}=J_1-J_2.\tag{2.32}$$

The generating functional for the three sources is then expressed as

$$\rho_\alpha(x,r,t;\mathbf{J})=\sqrt{\frac{1}{2\pi\langle q^2\rangle_g}}\exp\left[-\frac{1}{2\langle q^2\rangle_g}[r-r(t;\mathbf{J})]^2\right.$$
$$\left.-\frac{1}{2\hbar^2}\langle p^2\rangle_g x^2+\frac{i}{\hbar}p(t;\mathbf{J})x+\Xi(t;\mathbf{J})\right],\tag{2.33}$$

where

$$r(t;\mathbf{J})=\frac{i}{\hbar}\int_0^t dt' D^{(-+)}(t-t')J^{(+)}(t')+\frac{i}{\hbar}\int_0^t dt' D^{(--)}(t-t')J^{(-)}(t')+\frac{1}{\hbar}\int_0^{\beta\hbar} d\tau D^{(-3)}(t+i\tau)J_3(\tau), \tag{2.34}$$

$$p(t;\mathbf{J})=\frac{iM}{\hbar}\int_0^t dt' \dot{D}^{(-+)}(t-t')J^{(+)}(t')+\frac{iM}{\hbar}\int_0^t dt' \dot{D}^{(--)}(t-t')J^{(-)}(t')+\frac{M}{\hbar}\int_0^{\beta\hbar} d\tau \dot{D}^{(-3)}(t+i\tau)J_3(\tau), \tag{2.35}$$

$$\begin{aligned}\Xi(t;J)=&\frac{i}{\hbar}\int_0^t dt''[J_0(t'')-J_0'(t'')]-\frac{1}{\hbar^2}\int_0^t dt''\int_0^{t''} dt' J^{(-)}(t'')D^{(-+)}(t''-t')J^{(+)}(t')\\&-\frac{1}{2\hbar^2}\int_0^t dt''\int_0^t dt' J^{(-)}(t'')D^{(--)}(t''-t')J^{(-)}(t')+\frac{i}{\hbar^2}\int_0^t dt''\int_0^{\beta\hbar} d\tau J^{(-)}(t'')D^{(-3)}(t''+i\tau)J_3(\tau)\\&+\frac{1}{2\hbar^2}\int_0^{\beta\hbar} d\tau\int_0^{\beta\hbar} d\tau' J_3(\tau)D^{(33)}(\tau-\tau')J_3(\tau'),\end{aligned} \tag{2.36}$$

with

$$\begin{aligned}D^{(-+)}(t)\equiv&\langle q(t)q-qq(t)\rangle_g\\=&-\frac{i\hbar}{M}\int_{-\infty}^{\infty}\frac{d\omega}{\pi}\frac{\omega\tilde{\gamma}(\omega)}{(\omega_0^2-\omega^2)^2+\omega^2\tilde{\gamma}^2(\omega)}\\&\times\sin(\omega t),\end{aligned} \tag{2.37}$$

$$\begin{aligned}D^{(--)}(t)\equiv&\frac{1}{2}\langle q(t)q+qq(t)\rangle_g\\=&\frac{\hbar}{M}\int_{-\infty}^{\infty}\frac{d\omega}{2\pi}\frac{\omega\tilde{\gamma}(\omega)}{(\omega_0^2-\omega^2)^2+\omega^2\tilde{\gamma}^2(\omega)}\\&\times\coth\left(\frac{\beta\hbar\omega}{2}\right)\cos(\omega t),\end{aligned} \tag{2.38}$$

$$\begin{aligned}D^{(-3)}(t+i\tau)\equiv&\langle qq(t+i\tau)\rangle_g\\=&\frac{\hbar}{M}\int_{-\infty}^{\infty}\frac{d\omega}{2\pi}\frac{\omega\tilde{\gamma}(\omega)}{(\omega_0^2-\omega^2)^2+\omega^2\tilde{\gamma}^{\,2}(\omega)}\\&\times\left\{\coth\left(\frac{\beta\hbar\omega}{2}\right)\cos[\omega(t+i\tau)]\right.\\&\left.+i\sin[\omega(t+i\tau)]\right\},\end{aligned} \tag{2.39}$$

and

$$\begin{aligned}D^{(33)}(\tau)\equiv&\theta(\tau)\langle qq(-i\tau)\rangle_g+\theta(-\tau)\langle qq(i\tau)\rangle_g\\=&\frac{\hbar}{M}\int_{-\infty}^{\infty}\frac{d\omega}{2\pi}\frac{\omega\tilde{\gamma}(\omega)}{(\omega_0^2-\omega^2)^2+\omega^2\tilde{\gamma}^{\,2}(\omega)}\\&\times\left[\coth\left(\frac{\beta\hbar\omega}{2}\right)\cosh(\omega\tau)+\sinh(\omega\tau)\right],\end{aligned} \tag{2.40}$$

with

$$\tilde{\gamma}(\tilde{\omega})\equiv J(\omega)/\omega, \tag{2.41}$$

$$\langle q^2\rangle=D^{(--)}(0)=D^{(33)}(0),\quad \langle p^2\rangle=-M^2\ddot{D}^{(--)}(0). \tag{2.42}$$

As was shown in Ref. 30, the generating functional for the Liouville paths can be calculated by introducing the Liouville phase $\Phi_\alpha(t)$, the real force $F_\alpha^+(t)$, and the Liouville phase force $f_\alpha^-(t)$, which are defined by the harmonic parts of the time dependent potential, $U_L(t)$ and $U_R(t)$, as

$$\begin{aligned}\Phi_\alpha(t)=&-[U_L^0(r+x/2,t)-U_R^0(r-x/2,t)]|_{x=r=0},\\F_\alpha^+(t)=&-\left\{\frac{d}{dx}[U_L^0(r+x/2,t)-U_R^0(r-x/2,t)]\right\}\Big|_{x=r=0},\\f_\alpha^-(t)=&-\left\{\frac{d}{dr}[U_L^0(r+x/2,t)-U_R^0(r-x/2,t)]\right\}\Big|_{x=r=0}.\end{aligned} \tag{2.43}$$

Their explicit forms for a simple case [Eqs. (2.14) and (2.15)] are presented in Table II. The Liouville-space generating functional can be obtained from Eqs. (2.33)–(2.36) by simple replacements,

$$\begin{aligned}&J^{(+)}(t)\to F_\alpha^+(t)+J_\alpha^{(+)}(t),\quad J^{(-)}(t)\to f_\alpha^-(t)+J_\alpha^{(-)}(t),\\&J_0(t)-J_0'(t)\to\Phi_\alpha(t).\end{aligned} \tag{2.44}$$

The final results are given by

$$\rho_\alpha(x,r,t;\mathbf{J})=\sigma_\alpha(x,r,t;\mathbf{J})R_\alpha(t;\mathbf{J}), \tag{2.45}$$

where

$$\begin{aligned}\sigma_\alpha(x,r,t;\mathbf{J})=&\sqrt{\frac{1}{2\pi\langle q^2\rangle_g}}\exp\left\{-\frac{1}{2\langle q^2\rangle_g}\right.\\&\times[r-\langle\overline{r_t}\rangle_\alpha-r(t;\mathbf{J})]^2-\frac{1}{2\hbar^2}\langle p^2\rangle_g x^2\\&\left.+\frac{i}{\hbar}[\langle\overline{p_t}\rangle_\alpha-p(t;\mathbf{J})]x\right\}\end{aligned} \tag{2.46}$$

with

TABLE II. Functions $F_\alpha(s)$,$f_\alpha(s)$, and $\Phi_\alpha(s)$ for the paths given in Table I.

α	functions	$0\sim\tau_1$	$\tau_1\sim\tau_2$	$\tau_2\sim t$
1	$\Phi_1(s)$	0	$-\hbar(\omega_{eg}^0+\lambda)$	0
	$f_1(s)$	0	$-\hbar\xi$	0
	$F_1(s)$	0	$-\hbar\xi/2$	0
2	$\Phi_2(s)$	0	$-\hbar(\omega_{eg}^0+\lambda)$	0
	$f_2(s)$	0	$-\hbar\xi$	0
	$F_2(s)$	0	$-\hbar\xi/2$	$-\hbar\xi$

$$\langle \overline{r_t} \rangle_\alpha = \frac{i}{\hbar}\int_0^t dt' D^{(-+)}(t-t') F_\alpha^+(t') + \frac{i}{\hbar}\int_0^t dt' D^{(--)}(t-t') f_\alpha^-(t'), \tag{2.47}$$

and

$$\langle \overline{p_t} \rangle_\alpha = \frac{iM}{\hbar}\int_0^t dt' \dot{D}^{(-+)}(t-t') F_\alpha^+(t') + \frac{iM}{\hbar}\int_0^t dt' \dot{D}^{(--)}(t-t') f_\alpha^-(t'). \tag{2.48}$$

The function $R_\alpha(t;\mathbf{J})$ is expressed as

$$R_\alpha(t;\mathbf{J}) = \exp[Q_\alpha(t) + X_\alpha(t;\mathbf{J})], \tag{2.49}$$

where

$$Q_\alpha(t) = \frac{i}{\hbar}\int_0^t dt'' \left[\Phi_\alpha(t'') + \frac{i}{\hbar} f_\alpha^-(t'') \int_0^{t''} dt' D^{(-+)}(t''-t') F_\alpha^+(t') \right] - \frac{1}{2\hbar^2}\int_0^t dt'' \int_0^t dt' f_\alpha^-(t'') f_\alpha^-(t') D^{(--)}(t''-t'), \tag{2.50}$$

$$\begin{aligned} X_\alpha(t;\mathbf{J}) = {} & \frac{i}{\hbar}\int_0^t dt' \langle x_\alpha(t') \rangle J^{(+)}(t') + \frac{i}{\hbar}\int_0^t dt' \langle r_\alpha(t') \rangle J^{(-)}(t') + \frac{1}{\hbar}\int_0^{\beta\hbar} d\tau \langle \overline{q_\alpha}(t,\tau) \rangle J_3(\tau) \\ & - \frac{1}{\hbar^2}\int_0^t dt'' \int_0^{t''} dt' J^{(-)}(t'') D^{(-+)}(t''-t') J^{(+)}(t') \\ & - \frac{1}{2\hbar^2}\int_0^t dt'' \int_0^t dt' J^{(-)}(t'') D^{(--)}(t''-t') J^{(-)}(t') + \frac{i}{\hbar^2}\int_0^t dt'' \int_0^{\beta\hbar} d\tau J^{(-)}(t'') D^{(-3)}(t''+i\tau) J_3(\tau) \\ & + \frac{1}{2\hbar^2}\int_0^{\beta\hbar} d\tau \int_0^{\beta\hbar} d\tau' J_3(\tau) D^{(33)}(\tau-\tau') J_3(\tau'), \end{aligned} \tag{2.51}$$

with

$$\langle x_\alpha(t') \rangle = \frac{i}{\hbar}\int_{t'}^t dt'' f_\alpha^-(t'') D^{(-+)}(t''-t'),$$

$$\langle r_\alpha(t') \rangle = -\frac{i}{\hbar}\int_0^{t'} dt'' D^{(-+)}(t''-t') F_\alpha^+(t'') + \frac{i}{\hbar}\int_0^t dt'' f_\alpha^-(t'') D^{(--)}(t'-t''),$$

$$\langle \overline{q_\alpha}(t,\tau) \rangle = \frac{i}{\hbar}\int_0^t dt'' f_\alpha^-(t'') D^{(-3)}(t''+i\tau). \tag{2.52}$$

Using the generating functional Eqs. (2.45)–(2.52), the density matrix elements are now expressed as

$$\rho_\alpha(x,r,t) = \rho_\alpha(x,r,t;\mathbf{J})\big|_{J=0} - \left\{ \frac{i}{\hbar}\int_0^t dt' V_\alpha\left[\frac{\hbar}{i}\frac{\partial}{\partial J^{(+)}(t')}, \frac{\hbar}{i}\frac{\partial}{\partial J^{(-)}(t')}; t' \right] + \frac{1}{\hbar}\int_0^{\beta\hbar} d\tau V_g\left[\hbar\frac{\partial}{\partial J_3(\tau)} \right] \right\} \rho_\alpha(x,r,t;\mathbf{J}) \Big|_{\mathbf{J}=0}, \tag{2.53}$$

where $V_\alpha(x,r;t) \equiv V_L(r+x/2;t) - V_R(r-x/2;t)$. The normalized density matrix elements are defined as

$$\overline{\rho_\alpha}(x,r,t) = \frac{\rho_\alpha(x,r,t)}{\mathrm{tr}\{\rho_\alpha(x,r,0)\}}, \tag{2.54}$$

where $\rho_\alpha(x,r,t=0)$ corresponds to the equilibrium density matrix element including up to the first-order anharmonic perturbation.

III. *N*th ORDER RESPONSE FUNCTIONS FOR AN ANHARMONIC DISPLACED OSCILLATORS SYSTEM

We now specify the potentials. Hereafter we use dimensionless coordinates and momentum defined by

$$\sqrt{\frac{M\omega_0}{\hbar}} q \to q, \quad \sqrt{\frac{1}{M\hbar\omega_0}} p \to p, \tag{3.1}$$

respectively. Then the harmonic parts of the potential [Eq. (2.26)] are expressed as

$$U_g^0(q) \equiv \frac{\hbar\omega_0}{2} q^2, \quad U_e^0(q) = \frac{\hbar\omega_0}{2}(q-d)^2 + \hbar\omega_{eg}^0, \tag{3.2}$$

where $d = \sqrt{M\omega_0/\hbar D}$. We assume the following perturbation potentials:

$$V_g(q) \equiv \hbar\omega_0 \left(\frac{1}{3!} g_3 q^3 + \frac{1}{4!} g_4 q^4 \right) \equiv a_3 q^3 + a_4 q^4,$$

$$V_e(q)\equiv\hbar\omega_0\left[\frac{1}{2}g_2'(q-d)^2+\frac{1}{3!}g_3'(q-d)^3+\frac{1}{4!}g_4'(q-d)^4\right]$$
$$\equiv a_0'+a_1'q+a_2'q^2+a_3'q^3+a_4'q^4, \tag{3.3}$$

where

$$a_3=\frac{\hbar\omega_0 g_3}{3!},\quad a_4=\frac{\hbar\omega_0 g_4}{4!},$$
$$a_0'=\hbar\omega_0\left(\frac{g_2'd^2}{2}-\frac{g_3'd^3}{3!}+\frac{g_4'd^4}{4!}\right),$$
$$a_1'=\hbar\omega_0\left(-g_2'd+\frac{g_3'd^3}{2}-\frac{g_4'd^3}{3!}\right),$$
$$a_2'=\hbar\omega_0\left(\frac{g_2'}{2}-\frac{g_3'd}{2}+\frac{g_4'd^2}{4}\right),$$
$$a_3'=\hbar\omega_0\left(\frac{g_3'}{3!}-\frac{g_4'd}{3!}\right),\quad a_4'=\frac{\hbar\omega_0 g_4'}{4!}. \tag{3.4}$$

Note that, by introducing the perturbation term proportional to g_2', we can take into account the difference in the excited-state frequency, $\hbar\omega_0(1+g_2')$, compared to the ground-state one, ω_0. To write a result in compact form, it is convenient to introduce sign parameters $\epsilon_i=\pm$ for a time period $\tau_j<t<\tau_{j+1}$.[28] We chose $\epsilon_{2j-1}=+(-)$ as the $eg(ge)$ state for the odd time period, where a density matrix is in coherent states. In the same way, we chose $\epsilon_{2j}=+(-)$ as the $ee(gg)$ state for the even time period where a density matrix is in real states. Using the sign parameters, any process in the Nth order can be expressed by the set $\{\epsilon_j\}=\{\epsilon_1,\epsilon_2,\ldots,\epsilon_{N-1}\}$. The functions in Eq. (2.43) are then expressed as (see Ref. 30)

$$\Phi_\alpha(t)=-\hbar(\omega_{eg}^0+\lambda)\sum_{j=1}^{N/2}\epsilon_{2j-1}[\theta(t-\tau_{2j-1})-\theta(t-\tau_{2j})],$$
$$F_\alpha^+(t)=-\frac{\hbar\xi}{2}\left\{\theta(t-\tau_1)+\sum_{j=1}^{N/2}\epsilon_{2j}[\theta(t-\tau_{2j})-\theta(t-\tau_{2j+1})]\right\},$$
$$f_\alpha^-(t)=-\hbar\xi\sum_{j=1}^{N/2}\epsilon_{2j-1}[\theta(t-\tau_{2j-1})-\theta(t-\tau_{2j})], \tag{3.5}$$

where $\theta(t)$ is the step function and α now refers to the set $\{\epsilon_j\}$ and

$$\lambda\equiv\frac{d^2\omega_0}{2},\quad \xi=d\sqrt{\frac{M\omega_0^3}{\hbar}}=\frac{2\lambda}{d}\sqrt{\frac{\hbar}{M\omega_0}}. \tag{3.6}$$

Using the sign parameters ϵ_j, the time dependent potential for the Liouville proper path α can be expressed in center and difference coordinates as

$$V_\alpha(x,r;t)=V_L(r+x/2;t)-V_R(r-x/2;t)$$
$$=f_\alpha^0(t)+f_\alpha^1(t)r(t)+\tfrac{1}{2}F_\alpha^1(t)x(t)+\tfrac{1}{4}f_\alpha^2(t)x^2(t)+F_\alpha^2(t)x(t)r(t)+f_\alpha^2(t)r^2(t)+\tfrac{1}{8}F_\alpha^3(t)x^3(t)+\tfrac{3}{4}f_\alpha^3(t)x^2(t)r(t)$$
$$+\tfrac{3}{2}F_\alpha^3(t)x(t)r^2(t)+f_\alpha^3(t)r^3(t)+\tfrac{1}{16}f_\alpha^4(t)x^4(t)+\tfrac{1}{2}F_\alpha^4(t)x^3(t)r(t)+\tfrac{3}{2}f_\alpha^4(t)x^2(t)r^2(t)$$
$$+2F_\alpha^4(t)x(t)r^3(t)+f_\alpha^4(t)r^4(t). \tag{3.7}$$

The functions $f_\alpha^k(t)$ and $F_\alpha^k(t)[k=1-4]$ for the Liouville states corresponding to Eqs. (2.14) and (2.15) are given in Table II and expressed as

$$f_\alpha^k(t)=(a_k'-a_k)\sum_{j=1}^{N/2}\epsilon_{2j-1}[\theta(t-\tau_{2j-1})-\theta(t-\tau_{2j})],$$
$$F_\alpha^k(t)=(a_k'+a_k)\sum_{j=1}^{N/2}[\theta(t-\tau_{2j-1})-\theta(t-\tau_{2j})]+\sum_{j=1}^{N/2}[(1+\epsilon_{2j})a_k'+(1-\epsilon_{2j})a_k]\times[\theta(t-\tau_{2j})-\theta(t-\tau_{2j+1})], \tag{3.8}$$

where we set $a_0=a_1=a_2=0$.

The optical response can be expressed in terms of the optical polarization at the position $\mathbf{r}$ defined by

$$P(\mathbf{r},t)\equiv\mathrm{Tr}[\mu(|e\rangle\langle g|+|g\rangle\langle e|)\overline{\rho(t)}], \tag{3.9}$$

where the normalized density matrix, $\overline{\rho(t)}$, involves the interaction between the driving electric field, $[E(t)\equiv E(\mathbf{r},t)]$, and the system. If an interaction between the system and the electric field is weak, we may expand $\overline{\rho(t)}$ [see Eq. (2.10)] and consequently $P(\mathbf{r},t)$ in powers of the electric field. The Nth order optical process is calculated from the Nth response function, which is the $(N+1)$th time-correlation function of the dipole interaction. We can express any order of response function by using the Liouville path. The response function for the path α is expressed in the first order perturbation of Eq. (3.7) as

$$R_\alpha(t)=\mathrm{tr}\{\overline{\rho_\alpha}(t)\}=\int dr\,\overline{\rho_\alpha}(0,r;t), \tag{3.10}$$

where

$$R_\alpha(t)\equiv\left\{1-\frac{i}{\hbar}\int_0^t dt' V_\alpha\left[\frac{\hbar}{i}\frac{\partial}{\partial J^{(+)}(t')},\frac{\hbar}{i}\frac{\partial}{\partial J^{(-)}(t')};t'\right]-\frac{1}{\hbar}\int_0^{\beta\hbar}d\tau V_g\left[\hbar\frac{\partial}{\partial J_3(\tau)}\right]\right\}R_\alpha(t;\mathbf{J})\Big|_{\mathbf{J}=0},\quad(3.11)$$

since we found $\mathrm{tr}[\sigma_\alpha(x,r,t)]=1$ and $\mathrm{tr}[\rho_\alpha(x,r,t=0)]=1$, where

$$\sigma_\alpha(x,r,t)\equiv\sigma_\alpha(x,r,t;\mathbf{J})\big|_{\mathbf{J}=0}-\left\{\frac{i}{\hbar}\int_0^t dt' V_\alpha\left[\frac{\hbar}{i}\frac{\partial}{\partial J^{(+)}(t')},\frac{\hbar}{i}\frac{\partial}{\partial J^{(-)}(t')};t'\right]+\frac{1}{\hbar}\int_0^{\beta\hbar}d\tau V_g\left[\left|\hbar\frac{\partial}{\partial J_3(\tau)}\right|\right]\sigma_\alpha(x,r,t;\mathbf{J})\right|_{\mathbf{J}=0}.\quad(3.12)$$

After some calculations, we thus obtain

$$R_\alpha(t)=\left[1-\frac{i}{\hbar}\int_0^t dt' V_\alpha(t')-\frac{1}{\hbar}\int_0^{\beta\hbar}d\tau V_\alpha^g(t,\tau)\right]\times\exp[Q_\alpha(t)],\quad(3.13)$$

where

$$V_\alpha(t)=\sum_{j=1}^{N/2}V_\alpha^{2j-1}(t)[\theta(t-\tau_{2j-1})-\theta(t-\tau_{2j})]+\sum_{j=1}^{N/2-1}V_\alpha^{2j}(t)[\theta(t-\tau_{2j})-\theta(t-\tau_{2j-1})],\quad(3.14)$$

with

$$\begin{aligned}V_\alpha^{2j-1}(t)=&\epsilon_{2j-1}(a_0'+a_1'\langle r_\alpha(t)\rangle+a_2[\tfrac{1}{4}\langle x_\alpha(t)\rangle^2+\langle r_\alpha(t)\rangle^2+\langle q^2\rangle]\\&+(a_3'-a_3)[\tfrac{3}{4}\langle x_\alpha(t)\rangle^2\langle r_\alpha(t)\rangle+\langle r_\alpha(t)\rangle^3+3\langle q^2\rangle\langle r_\alpha(t)\rangle]\\&+(a_4'-a_4)\{\tfrac{1}{16}\langle x_\alpha(t)\rangle^4+\langle r_\alpha(t)\rangle^4+6\langle q^2\rangle\langle r_\alpha(t)\rangle^2+3\langle q^2\rangle^2\\&+\tfrac{3}{2}[\langle x_\alpha(t)\rangle^2\langle r_\alpha(t)\rangle^2+\langle q^2\rangle\langle x_\alpha(t)\rangle^2]\})+\tfrac{1}{2}a_1'\langle x_\alpha(t)\rangle+a_2'\langle x_\alpha(t)\rangle\langle r_\alpha(t)\rangle\\&+(a_3'+a_3)\{\tfrac{1}{8}\langle x_\alpha(t)\rangle^3+\tfrac{3}{2}[\langle x_\alpha(t)\rangle\langle r_\alpha(t)\rangle^2+\langle q^2\rangle\langle x_\alpha(t)\rangle]\}\\&+(a_4'+a_4)\{\tfrac{1}{2}\langle x_\alpha(t)\rangle^3\langle r_\alpha(t)\rangle+2[\langle x_\alpha(t)\rangle\langle r_\alpha(t)\rangle^3+3\langle q^2\rangle\langle x_\alpha(t)\rangle\langle r_\alpha(t)\rangle]\},\end{aligned}\quad(3.15)$$

$$\begin{aligned}V_\alpha^{2j}(t)=&\tfrac{1}{2}[(1+\epsilon_{2j})a_1'+(1-\epsilon_{2j})a_1]\langle x_\alpha(t)\rangle+[(1+\epsilon_{2j})a_2'+(1-\epsilon_{2j})a_2]\langle x_\alpha(t)\rangle\langle r_\alpha(t)\rangle\\&+[(1+\epsilon_{2j})a_3'+(1-\epsilon_{2j})a_3]\{\tfrac{1}{8}\langle x_\alpha(t)\rangle^3+\tfrac{3}{2}[\langle x_\alpha(t)\rangle\langle r_\alpha(t)\rangle^2+\langle q^2\rangle\langle x_\alpha(t)\rangle]\}\\&+[(1+\epsilon_{2j})a_4'+(1-\epsilon_{2j})a_4]\{\tfrac{1}{2}\langle x_\alpha(t)\rangle^3\langle r_\alpha(t)\rangle+2[\langle x_\alpha(t)\rangle\langle r_\alpha(t)\rangle^3+3\langle q^2\rangle\langle x_\alpha(t)\rangle\langle r_\alpha(t)\rangle]\},\end{aligned}\quad(3.16)$$

and

$$V_\alpha^g(t,\tau)=\frac{g_3}{3!}[\langle\overline{q_\alpha}(t,\tau)\rangle^3+3\langle q^2\rangle\langle\overline{q_\alpha}(t,\tau)\rangle]+\frac{g_4}{4!}[\langle\overline{q_\alpha}(t,\tau)\rangle^4+6\langle q^2\rangle\langle\overline{q_\alpha}(t,\tau)\rangle^2+3\langle q^2\rangle^2].\quad(3.17)$$

Here, $\langle x_\alpha(t)\rangle$, $\langle r_\alpha(t)\rangle$, and $\langle q_\alpha(t,\tau)\rangle$ are defined by Eq. (2.52).

IV. FIRST-, THIRD-, AND FIFTH-ORDER POLARIZATIONS AND RESPONSE FUNCTIONS

Using the previous results, we present here the first-, third-, and fifth polarizations in terms of response functions.

A. First-order polarization

Hereafter, we use the time variable $t_k=\tau_{k+1}-\tau_k$ and $t_{jk}=\tau_{j+1}-\tau_k$. The first order polarization is then expressed as

$$P^{(1)}(\mathbf{r},t)=-\frac{i}{\hbar}\int_0^\infty dt_1 E(\mathbf{r},t-t_1)\sum_{\epsilon_1=\pm}R_{\epsilon_1}(t_1),\quad(4.1)$$

where the first-order response function is

$$R_{\epsilon_1}(t_1)=\left[1-\frac{i}{\hbar}\int_0^{t_1}dt' V_{\epsilon_1}^1(t')-\frac{1}{\hbar}\int_0^{\beta\hbar}d\tau V_{\epsilon_1}^g(t_1,\tau)\right]\exp[Q_{\epsilon_1}(t_1)],\quad(4.2)$$

in which

$$Q_{\epsilon_1}(t)=-i\epsilon_1\omega_{eg}t_1-g_{-\epsilon_1}(t_1),\quad(4.3)$$

with

$$\omega_{eg} \equiv \omega_{eg}^0 + \lambda. \tag{4.4}$$

The perturbation functions, V_α^1 and V_α^g are given by Eq. (3.15) with

$$\langle x_\alpha(t'')\rangle = 2\epsilon_1 \xi^{-1} \dot{g}''(t_1 - t''), \tag{4.5}$$

$$\langle r_\alpha(t'')\rangle = -i\xi^{-1}[\epsilon_1 \dot{g}_{\epsilon_0\epsilon_1}(t'') + \epsilon_1 \dot{g}'(t_1 - t'')], \tag{4.6}$$

and by Eq. (3.17) with

$$\langle \overline{q_\alpha}(t_1, \overline{\tau})\rangle = i\xi^{-1}\epsilon_1 \dot{g}_3(t_1, i\overline{\tau}), \tag{4.7}$$

respectively. In the above we defined

$$g_\pm(t) = \xi^2 \int_0^t dt' \int_0^{t'} dt''[D^{(--)}(t'') \mp \tfrac{1}{2} D^{(-+)}(t'')]$$

$$\equiv g'(t) \mp i g''(t), \tag{4.8}$$

and

$$g_3(t, i\tau) = \xi^2 \int_0^t dt' \int_0^{t'} dt'' D^{(-3)}(t'' + i\tau). \tag{4.9}$$

B. Third-order polarization

Next we present third-order polarization, which has numerous applications to ultrafast laser techniques, such as pump–probe and photon echo. The result is expressed as

$$P^{(3)}(\mathbf{r},t) = \frac{i}{\hbar^3} \int_0^\infty dt_3 \int_0^\infty dt_2 \int_0^\infty dt_1 E(\mathbf{r}, t - t_3)$$

$$\times E(\mathbf{r}, t - t_2 - t_3) E(\mathbf{r}, t - t_1 - t_2 - t_3)$$

$$\times \sum_{\epsilon_1, \epsilon_2, \epsilon_3 = \pm} R_{\epsilon_1\epsilon_2\epsilon_3}(t_3, t_2, t_1), \tag{4.10}$$

where

$$R_{\epsilon_1\epsilon_2\epsilon_3}(t_1, t_2, t_3)$$

$$= \left\{ 1 - \frac{i}{\hbar} \left[\int_0^{t_1} dt' V^1_{\epsilon_1\epsilon_2\epsilon_3}(t') + \int_{t_1}^{t_{12}} dt' V^2_{\epsilon_1\epsilon_2\epsilon_3}(t') \right.\right.$$

$$\left.\left. + \int_{t_{12}}^{t_{13}} dt' V^3_{\epsilon_1\epsilon_2\epsilon_3}(t') \right] - \frac{1}{\hbar} \int_0^{\beta\hbar} d\tau V^g_{\epsilon_1\epsilon_2\epsilon_3}(\tau) \right\}$$

$$\times \exp[Q_{\epsilon_1\epsilon_2\epsilon_3}(t_1, t_2, t_3)]. \tag{4.11}$$

Here,

$$Q_{\epsilon_1\epsilon_2\epsilon_3}(t_1, t_2, t_3) = -i\omega_{eg}(\epsilon_1 t_1 + \epsilon_3 t_3) - g_{-\epsilon_1}(t_1)$$

$$- g_{\epsilon_2\epsilon_3}(t_3) - \epsilon_1\epsilon_3[g_{\epsilon_1\epsilon_2}(t_2)$$

$$- g_{\epsilon_1\epsilon_2}(t_{23}) - g_{-\epsilon_1}(t_{12}) + g_{-\epsilon_1}(t_{13})], \tag{4.12}$$

and $V^j_{\epsilon_1\epsilon_2\epsilon_3}(t')$ and $V^g_{\epsilon_1\epsilon_2\epsilon_3}(\tau)$ are defined by Eqs. (3.15) and (3.16) with

$$\langle x_{\epsilon_1\epsilon_2\epsilon_3}(t')\rangle = 2\xi^{-1}\{\epsilon_1 \theta(t_1 - t')\dot{g}''(t_1 - t')$$

$$- \epsilon_3[\theta(t_{12} - t')\dot{g}''(t_{12} - t') - \dot{g}''(t_{13} - t')]\},$$

$$\langle r_{\epsilon_1\epsilon_2\epsilon_3}(t')\rangle = -i\xi^{-1}\{\epsilon_1 \theta(t_1 - t')\dot{g}'(t_1 - t')$$

$$- \epsilon_3[\theta(t_{12} - t')\dot{g}'(t_{12} - t') - \dot{g}'(t_{13} - t')]\}$$

$$- i\xi^{-1}\{\epsilon_1[\dot{g}_{-\epsilon_1}(t') - \theta(t' - t_1)\dot{g}_{\epsilon_1\epsilon_2}(t' - t_1)]$$

$$+ \epsilon_3 \theta(t' - t_{12})\dot{g}_{\epsilon_2\epsilon_3}(t' - t_{12})\}, \tag{4.13}$$

and Eq. (3.17) with

$$\langle \overline{q_{\epsilon_1\epsilon_2\epsilon_3}}(t_1, t_2, t_3, \tau)\rangle = i\xi^{-1}\{\epsilon_1 \dot{g}_3(t_1, i\tau)$$

$$+ \epsilon_3[\dot{g}_3(t_{13}, i\tau) - \dot{g}_3(t_{12}, i\tau)]\}. \tag{4.14}$$

C. Fifth-order polarization

Here, we present fifth-order polarization. As we will show in the next section, anharmonicity plays a central role in this order. The polarization is expressed as

$$P^{(5)}(\mathbf{r},t) = \left(-\frac{i}{\hbar}\right)^5 \left(\prod_{k=1}^5 \int_0^\infty dt_k\right) \left[\prod_{k=1}^5 E\left(\mathbf{r}, t - \sum_{m=1}^k t_m\right)\right]$$

$$\times \sum_{\{\epsilon;5\}=\pm} R_{\{\epsilon;5\}}(t_1, t_2, t_3, t_4, t_5), \tag{4.15}$$

where

$$R_{\{\epsilon;5\}}(t_1, t_2, t_3, t_4, t_5) = \left[1 - \frac{i}{\hbar} \sum_{j=1}^5 \int_{t_{1,j-I}}^{t_{1,j}} dt' V^j_{\{\epsilon;5\}}(t') \right.$$

$$\left. - \frac{1}{\hbar} \int_0^{\beta\hbar} d\tau V^g_{\{\epsilon;5\}}(\tau) \right]$$

$$\times \exp[Q_{\{\epsilon;5\}}(t_1, t_2, t_3, t_4, t_5)], \tag{4.16}$$

in which $t_{10} = 0$ and $\{\epsilon;N\}$ refers to the set $\{\epsilon_1, \epsilon_2, \ldots, \epsilon_N\}$ and

$$Q_{\{\epsilon\}}(t_1, t_2, t_3, t_4, t_5) = -i\omega_{eg}(\epsilon_1 t_1 + \epsilon_3 t_3 + \epsilon_5 t_5) - g_{-\epsilon_1}(t_1) - g_{\epsilon_2\epsilon_3}(t_3) - g_{\epsilon_4\epsilon_5}(t_5)$$

$$- \epsilon_1\epsilon_3[g_{\epsilon_1\epsilon_2}(t_2) - g_{\epsilon_1\epsilon_2}(t_2 + t_3) - g_{-\epsilon_1}(t_{12}) + g_{-\epsilon_1}(t_{13})] - \epsilon_1\epsilon_5[g_{\epsilon_1\epsilon_2}(t_{24}) - g_{\epsilon_1\epsilon_2}(t_{25}) - g_{-\epsilon_1}(t_{14})$$

$$+ g_{-\epsilon_1}(t_{15})] - \epsilon_3\epsilon_5[g_{\epsilon_3\epsilon_4}(t_4) - g_{\epsilon_3\epsilon_4}(t_{45}) - g_{\epsilon_2\epsilon_3}(t_{34}) + g_{\epsilon_2\epsilon_3}(t_{35})]. \tag{4.17}$$

The functions $V^j_{\{\epsilon;5\}}$ and $V^g_{\{\epsilon;5\}}$ are defined by Eqs. (3.15) and (3.16) with

$$\langle x_{\{\epsilon;5\}}(t')\rangle = 2\xi^{-1}\{\epsilon_1\theta(t_1-t')\dot{g}''(t_1-t') - \epsilon_3[\theta(t_{12}-t')\dot{g}''(t_{12}-t') - \theta(t_{13}-t')\dot{g}''(t_{13}-t')] - \epsilon_5[\theta(t_{14}-t')\dot{g}''(t_{14}-t') - \dot{g}''(t_{15}-t')]\}, \tag{4.18}$$

$$\langle r_{\{\epsilon;5\}}(t')\rangle = -i\xi^{-1}\{\epsilon_1[\dot{g}_{-\epsilon_1}(t') - \theta(t'-t_1)\dot{g}_{\epsilon_1\epsilon_2}(t'-t_1)] + \epsilon_3[\theta(t'-t_{12})\dot{g}_{\epsilon_2\epsilon_3}(t'-t_{12}) - \theta(t'-t_{13})\dot{g}_{\epsilon_3\epsilon_4}(t'-t_{13})] + \epsilon_5\theta(t'-t_{14})\dot{g}_{\epsilon_4\epsilon_5}(t'-t_{14})\} - i\xi^{-1}\{\epsilon_1\theta(t_1-t')\dot{g}'(t_1-t') - \epsilon_3[\theta(t_{12}-t')\dot{g}'(t_{12}-t') - \theta(t_{13}-t')\dot{g}'(t_{13}-t')] - \epsilon_5[\theta(t_{14}-t')\dot{g}'(t_{14}-t') - \dot{g}'(t_{15}-t')]\}, \tag{4.19}$$

and Eq. (3.17) with

$$\langle \overline{q_{\{\epsilon;5\}}}(t_1,t_2,t_3,t_4,t_5,\tau)\rangle = i\xi^{-1}\{\epsilon_1\dot{g}_3(t_1,i\tau) + \epsilon_3[\dot{g}_3(t_{13},i\tau) - \dot{g}_3(t_{12},i\tau)] + \epsilon_5[\dot{g}_3(t_{15},i\tau) - \dot{g}_3(t_{14},i\tau)]\}. \tag{4.20}$$

V. LINEAR ABSORPTION, PUMP–PROBE, AND PHOTON ECHO SPECTROSCOPIES IN THE ANHARMONIC DISPLACED OSCILLATORS SYSTEM

Numerous applications to frequency-domain and time-domain ultrafast techniques have been found for the first and third order response functions, $R_\epsilon(t_1)$ and $R_{\{\epsilon;3\}}(t_1,t_2,t_3)$, for harmonic potential systems. The present results provide a generalization to anharmonic potential surfaces.

In the following, we assume the Ohmic spectral distribution, $J(\omega)=\gamma\omega$,[28] where analytical expressions of symmetrized and antisymmetrized correlation functions are known.[42] The auxiliary function is then given by

$$g_\pm(t) = g'(t) \pm ig''(t), \tag{5.1}$$

where

$$g'(t) = \lambda\left\{\left[\frac{\lambda_1^2}{2\zeta\omega_0^2}(e^{-\lambda_2 t}+\lambda_2 t-1)\coth\left(\frac{i\beta\hbar\lambda_2}{2}\right) - \frac{\lambda_2^2}{2\zeta\omega_0^2}(e^{-\lambda_1 t}+\lambda_1 t-1)\coth\left(\frac{i\beta\hbar\lambda_1}{2}\right)\right] - \frac{4\gamma\omega_0^2}{\beta\hbar}\sum_{n=1}^{\infty}\frac{1}{\nu_n}\frac{e^{-\nu_n t}+\nu_n t-1}{(\omega_0^2+\nu_n^2)^2-\gamma^2\nu_n^2}\right\}, \tag{5.2}$$

and

$$ig''(t) = i\lambda\left\{e^{-\gamma t/2}\left[\frac{\gamma^2/2-\omega_0^2}{\zeta\omega_0^2}\sin(\zeta t) + \frac{\gamma}{\omega_0^2}\cos(\zeta t)\right] + t - \frac{\gamma}{\omega_0^2}\right\}. \tag{5.3}$$

In the above, we have used the definitions, $\nu_n = 2\pi n/\hbar\beta$, and

$$\lambda_1 = \frac{\gamma}{2} + i\zeta, \quad \lambda_2 = \frac{\gamma}{2} - i\zeta, \quad \zeta = \sqrt{\omega_0^2 - \gamma^2/4}. \tag{5.4}$$

To carry out a numerical calculation, the frequency of the unperturbed potential, the damping, the dimensionless displacement and the temperature are taken to be, $\omega_0 = 600(\mathrm{cm}^{-1})$, $\gamma = 40(\mathrm{cm}^{-1})$, $d=1.0$, and $T=300(\mathrm{K})$, respectively.

A. Linear absorption spectroscopy

As a simple application of these results we first calculated the linear absorption spectrum given by

$$I(\omega) = \int_0^\infty dt R_+(t)\exp(i\omega t) + \text{c.c.} \tag{5.5}$$

To check the validity of the perturbative approximation [Eq. (4.2)], we have compared the linear absorption spectra, calculated from the present formula, with ones from the multistate Fokker–Planck equation. (This Fokker–Planck approach can be used for a system with any shape of potentials at a relatively high temperature.[26]) We found that our expressions are valid for $g_3, g_4, g_3', g_4' < 0.1$ at room temperature, for $\omega_0 = 600(\mathrm{cm}^{-1})$. These anharmonic parameters can be made larger for lower temperatures, since, in such a case, the initial distribution of the wave packet is concentrated at the bottom of the potential, where the anharmonicity plays a minor role. Note that, as we have mentioned in Sec. I, calculating higher-order response functions using the equations of motion approach is not an easy task and we have checked the validity of our approximation only for the linear absorption spectrum.

Figure 2 shows the linear absorption spectra calculated using Eq. (5.5) for different anharmonicities; (1) the harmonic ($g_j=0$ and $g_j'=0$); (2) the ground-state cubic perturbation ($g_j=0$ and $g_j'=0$, except $g_3=-0.08$); (3) the ground-state quadratic perturbation case ($g_j=0$ and $g_j'=0$, except $g_4=0.08$); (4) the excited-state cubic perturbation ($g_j=0$ and $g_j'=0$, except $g_3'=-0.08$); and (5) the excited-state quadratic perturbation ($g_j=0$ and $g_j'=0$, except $g_4'=0.08$). As a reference, we have presented the spectrum for (1), the harmonic case, both in Figs. 2(a) and 2(b). Here, we set detuning $\Delta\omega = \omega - \omega_{eg}$. As can be seen from Fig. 2, the heights of the phonon lines increase for (2), the ground-state cubic perturbation case, whereas they decrease for (4), the excited-state cubic perturbation case. The physical essence of the phenomenon is as follows: cubic anharmonicity shifts the center of the wave packet, located at the bottom of the potential, towards the positive direction of the nuclear coordinate (see the ground-state potential in Fig. 1). This shift effectively decreases the displacement, d, for (2),

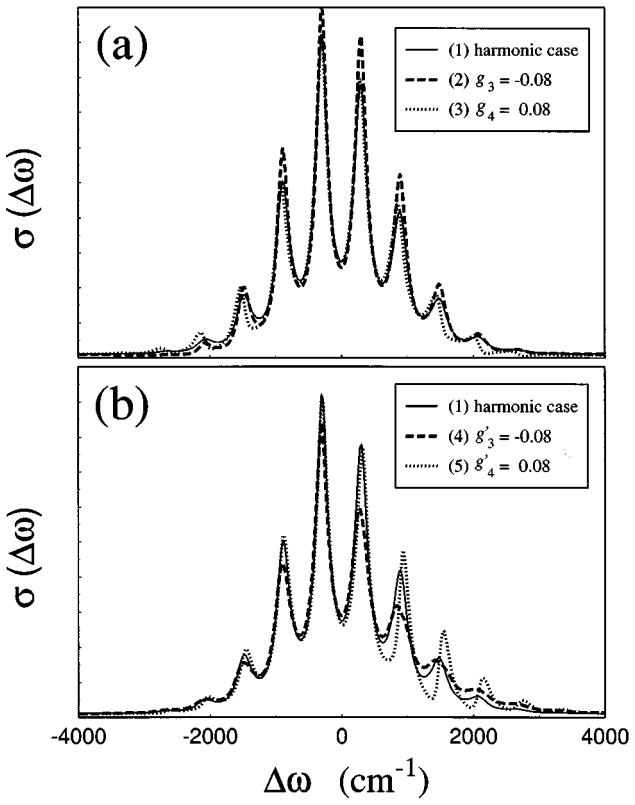

FIG. 2. Absorption spectra for different anharmonicities; (1) the harmonic case ($g_j=0$ and $g'_n=0$); (2) the ground-state cubic case ($g_3=-0.08$); (3) the ground-state quadratic case ($g_4=0.08$); (4) the excited-state cubic case ($g'_3=-0.08$); and (5) the excited-state quadratic case ($g'_4=0.08$).

whereas it increases for (4). For a small displacement, equivalent to case (2), electronically near resonant transitions, such as $1\rightarrow 0,\ 0\rightarrow 0,\ 0\rightarrow 1$, are the main contribution to the spectrum. For a large displacement, equivalent to case (4), the electronically off-resonant transitions, such as $3\rightarrow 0,\ 2\rightarrow 0,\ 0\rightarrow 2,\ 0\rightarrow 3$ can also take part so the spectrum is spread out over a broader frequency range. Thus, the heights of the phonon lines increase for (2), whereas they decrease for (4).

In the quadratic anharmonicity case, the phonon lines shift to the red, compared with the harmonic one, for (3), the ground-state quadratic perturbation, whereas they shift to the blue, for (5), the excited-state quadratic perturbation. This is because the quadratic perturbation increases the eigenenergy of the phonon bands. As a result, the perturbation of the ground-state potential decreases the transition frequencies between $|g\rangle$ and $|e\rangle$, while the perturbation on the excited-state increases them. Note that, at this temperature, most population is in the vibrational ground state for (3), however, the anharmonicity can increase the zero point energy and, thus, we observed the shift of phonon lines even in such a case.

B. Impulsive pump–probe spectroscopy

In a pump–probe experiment, the system is first subjected to a short pump pulse, then after a delay, τ, a second probe pulse interacts with the system. The external electric field is given by

$$E(\mathbf{r},t)=E_1(t+\tau)\exp(i\mathbf{k_1}\mathbf{r}-i\Omega_1 t)+E_2(t)\exp(i\mathbf{k_2}\mathbf{r}-i\Omega_2 t)+\text{c.c.}, \tag{5.6}$$

where $E_1(t)$, $\mathbf{k}_1$, and Ω_1 are the temporal envelopes, the wave vector, and the center frequency of the pump field, and $E_2(t)$, $\mathbf{k}_2$, and Ω_2 are those of the probe field, respectively. The difference absorption spectrum is[9]

$$S_{IPP}(\Omega_1,\Omega_2;\omega_2,\tau)=-2\ \mathrm{Im}E_2(\omega_2)P^{(3)}_{k_2}(\omega_2), \tag{5.7}$$

where

$$E_2(\omega_2)=\frac{1}{\sqrt{2\pi}}\int_{-\infty}^{\infty}dt\exp[i(\omega_2-\Omega_2)t]E_2(t), \tag{5.8}$$

and

$$P^{(3)}_{k_2}(\omega_2)=\frac{1}{\sqrt{2\pi}}\int_{-\infty}^{\infty}dt\exp[i(\omega_2-\Omega_2)t]P^{(3)}_{k_2}(t). \tag{5.9}$$

In the impulsive limit, the pump and probe pulses are short compared to the dynamical time scales of the potential and we can assume that[35,43]

$$E_1(t)=\theta_1\delta(t),\quad E_2(t)=\theta_2\delta(t), \tag{5.10}$$

where θ_1 and θ_2 are the pump and pulse areas, respectively. For the impulsive pump case, $R_{+++}(t,\tau,0)=R_{-++}(t,\tau,0)$ and $R_{--+}(t,\tau,0)=R_{+-+}(t,\tau,0)$, so we have

$$S_{IPP}(\omega_2-\Omega_2)=2\ \mathrm{Re}\int_0^{\infty}dt\exp[i(\omega_2-\Omega_2)t]\times[R_{-++}(t,\tau,0)+R_{--+}(t,\tau,0)]. \tag{5.11}$$

Here, we set $\mu\theta_1=\mu\theta_2=1$.

We have calculated the impulsive pump–probe spectrum for different pump–probe delay periods, τ, with detuning, $\Delta\omega=\omega_2-\Omega_2-\omega_{eg}$, for the cases discussed in Sec. V A. Figure 3 shows the impulsive pump–probe spectrum for (1), the harmonic case. Because the pump pulse is short compared with the period of the underdamped modes, it creates a vibrational coherence in the excited electronic state. As a result, the heights of the peaks show a quantum beat oscillation as a function of delay time. Figures 4, 5, and 6 show the pump–probe spectra for cases (2), (4), and (5), respectively. Since the profile of signals for case (3) is very similar to those of the harmonic ones, we do not display their results again. Pump–probe spectra in the anharmonic cases show behavior similar to those of the linear absorption cases, except that the peaks show quantum beat oscillations corresponding to the movement of the wave packet created in the excited state. In principle, the effects of anharmonicity must be larger for higher-order optical processes, since the laser

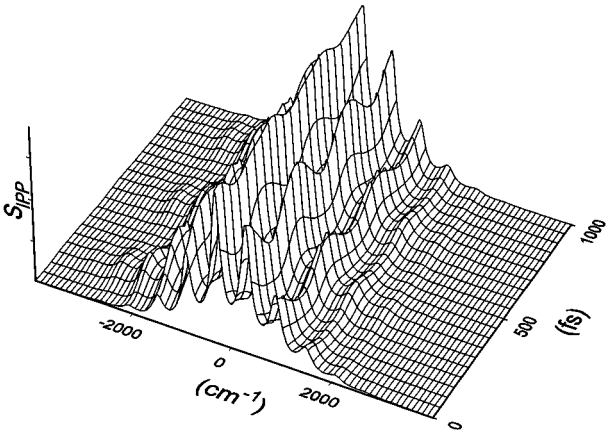

FIG. 3. The impulsive pump–probe spectrum as a function of time delay, τ, and wavelength, $\Delta\omega=\omega_2-\Omega_2-\omega_{eg}$, for (1) the harmonic case ($g_j=0$ and $g_j'=0$).

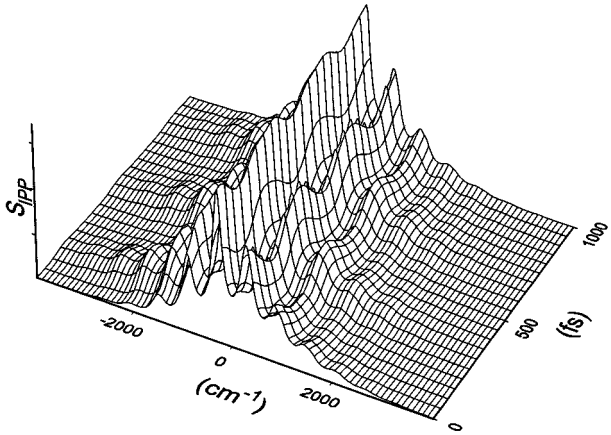

FIG. 5. The impulsive pump–probe spectrum for (4) the excited-state cubic perturbation case ($g_3'=-0.08$).

can interact with the potentials many times. However, we could not observe any clear effect of anharmonicity in the pump–probe experiments compared with the linear absorption spectrum.

C. Impulsive photon echo

In a photon echo experiment, the molecular system is subjected to two short pulses each with a wave vector $\mathbf{k}_1$ and $\mathbf{k}_2$, separated by a delay τ [see Eq. (5.6)]. The first pulse creates a coherence between states $|g\rangle$ and $|e\rangle$. The total polarization immediately begins to dephase, due to a variety of factors including pure dephasing, inhomogeneous distribution of resonant frequencies, and anharmonicity of vibrational modes. The second pulse arrives at a variable delay time, τ, after the first pulse, and interacts twice with the sample. When the pulses are short compared with the dynamical time scales of the heat-bath, the photon echo signal, emitted in the direction $2\mathbf{k}_2-\mathbf{k}_1$ is given by[9]

$$S_{IPE}(\tau,t)=|P^{(3)}_{2\mathbf{k}_2-\mathbf{k}_1}(t)|^2 =|R_{-++}(\tau,0,t)+R_{--+}(\tau,0,t)|^2, \tag{5.12}$$

where the argument t refers to the detection time of the signal. The second pulse causes a rephasing of the inhomogeneous-broadening contribution, which is simulated by the additional overdamped oscillator mode, to the linewidth at $\tau=t$, so we can observe the homogeneous contribution as the echo signal.[43] Here, we derive the shape of the echo decay in the presence of the anharmonicity. Figures 7–10 display the photon echo signal calculated from Eq. (5.12) for differing anharmonicities. Photon echo techniques have been used to separate the homogeneous contribution of the linewidth from the inhomogeneous ones. We have not included the inhomogeneous contributions here, since these experiments may be used to obtain information about anharmonicity in the system without inhomogeneity. {The inhomogeneous contribution can be included in our result by multiplying Eq. (5.12) by the factor $\exp[\Delta^2(t-\tau)^2]$}. Figure 7 is for (1), the harmonic case and here we see an initial decay followed by oscillations. These are quantum beats, resulting

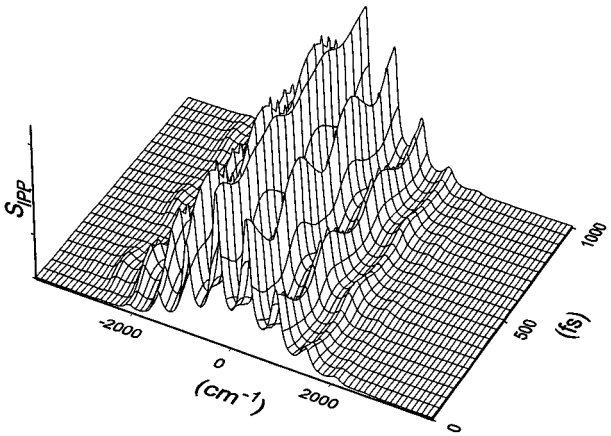

FIG. 4. The impulsive pump–probe spectrum for (2) the ground-state cubic perturbation case ($g_3=-0.08$).

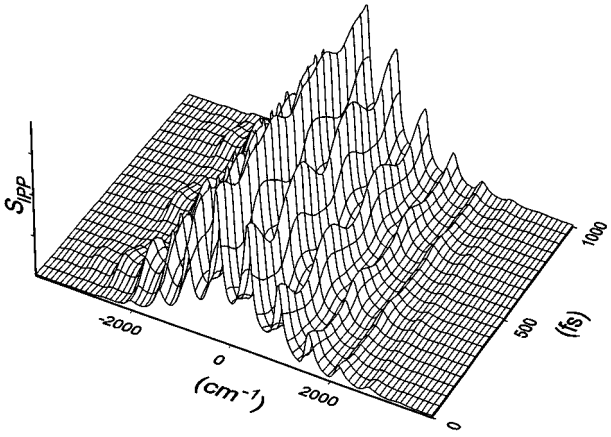

FIG. 6. The impulsive pump–probe spectrum for (5) the excited-state quadratic perturbation case ($g_4'=-0.08$).

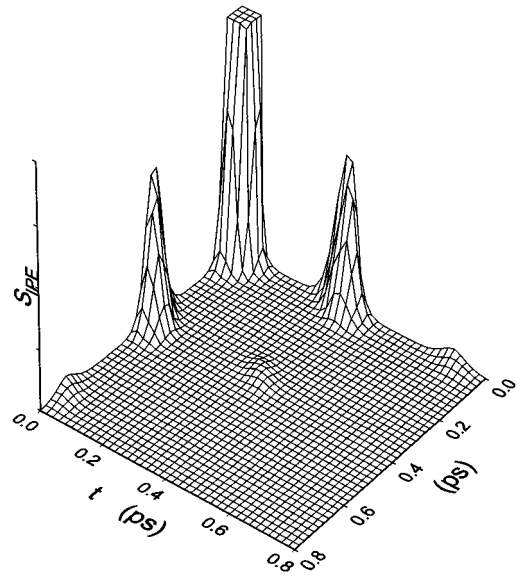

FIG. 7. The impulsive photon echo signal plotted as a function of t and τ for (1) the harmonic case ($g_j=0$ and $g_j'=0$). The free induction decay peak at $t=0$ and $\tau=0$ has been cut off to show the subsequent peaks better; it is approximately 20 times higher than is shown in the figure.

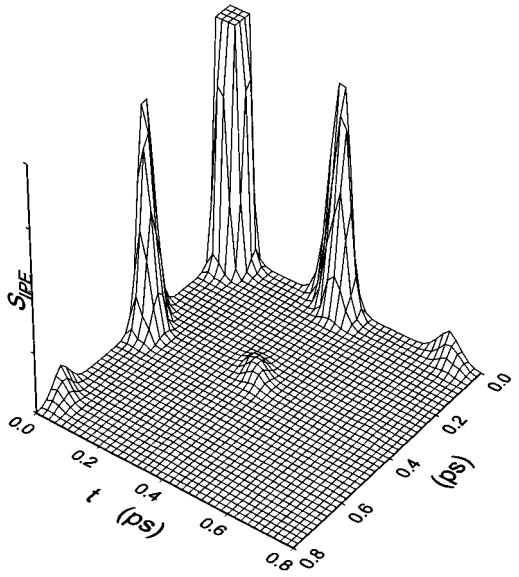

FIG. 8. The impulsive photon echo signal for (2) the ground-state cubic perturbation case ($g_3=-0.08$). The free induction decay peak is approximately 20 times higher than is shown in the figure.

from the modulation of the electronic polarization by a vibronic oscillation with frequency $\omega_0=600(\mathrm{cm}^{-1})$. The photon echo signal corresponds to the peak along the $\tau=t$ line. The peaks around $(\tau,t)=(0.35,\ 0)$, $(0.7,0)$, $(0,0.35)$, and $(0,0.7)$ (ps) would not be observed if inhomogeneity were present. Figure 8 is for (2), the ground-state cubic perturbation case. The height of the peaks increases, because the transitions between $|g\rangle$ and $|e\rangle$ (such as 0–0, 2–0 transitions) have increased due to the anharmonicity, as seen in Fig. 2(a). In contrast, the height of the peaks decreases in Fig. 9, for (3), the excited-state cubic perturbation case, since the transitions decrease in this case as seen in Fig. 2(b). Figure 10 is for (5), the excited-state quadratic perturbation case. In this case, the heights of the peaks have increased because the transitions far from resonance (such as 0–0, 0–2, and 0–3) have increased. In principle, anharmonicity causes the oscillation frequency to deviate from that of a harmonic oscillator, and this may make the width of the peaks broader. However, since here we have only considered a very small deformation of potential, we have not observed such effects.

VI. TWO-DIMENSIONAL RESONANT SPECTROSCOPY FOR AN ANHARMONIC DISPLACED OSCILLATOR SYSTEM

The contribution of anharmonicity, in the experiments we have studied so far, do not show major effects of anharmonicity. This is because we have only considered very weak anharmonicity. We propose here two-dimensional resonant spectroscopy (2DRS), which can provide clear signatures of anharmonicity, although this may still be weak in some cases.

We consider an experiment in which $E(t)$ consists of a train of three resonant laser pulses. The response of the system is detected through an additional probe pulse $E_f(t)$. The configuration of laser pulses is shown in Fig. 11. The external field is expressed as

$$\begin{aligned} E(\mathbf{r},t)=&E_1(t)e^{i\mathbf{k_1}\mathbf{r}-i\Omega_1 t}+E_1'(t)e^{i\mathbf{k}_1'\mathbf{r}-i\Omega_1' t}\\ &+E_2(t-T_1)e^{i\mathbf{k_2}\mathbf{r}-i\Omega_2 t}+E_2(t-T_1)'e^{i\mathbf{k}_2'\mathbf{r}-i\Omega_2' t}\\ &+E_3(t-T_1-T_2)e^{i\mathbf{k_3}\mathbf{r}-i\Omega_3 t}\\ &+E_f(t-T_1-T_2-\delta)e^{-i\mathbf{k_f}\mathbf{r}+i\Omega_f t+\phi}+\text{c.c.} \end{aligned} \tag{6.1}$$

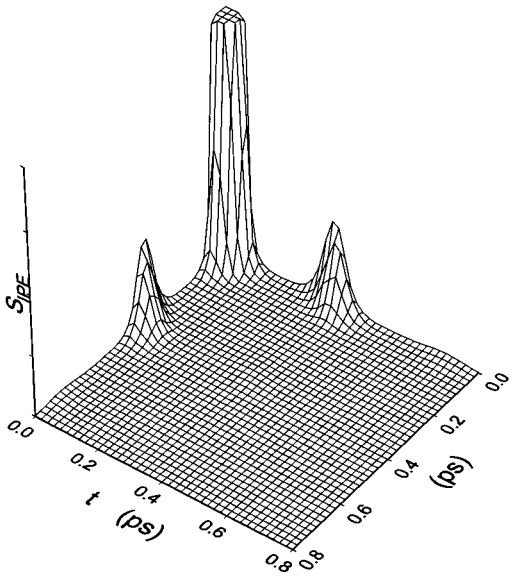

FIG. 9. The impulsive photon echo signal for (4) the excited-state cubic perturbation case ($g_3'=-0.08$). The free induction decay peak is approximately 20 times higher than is shown in the figure.

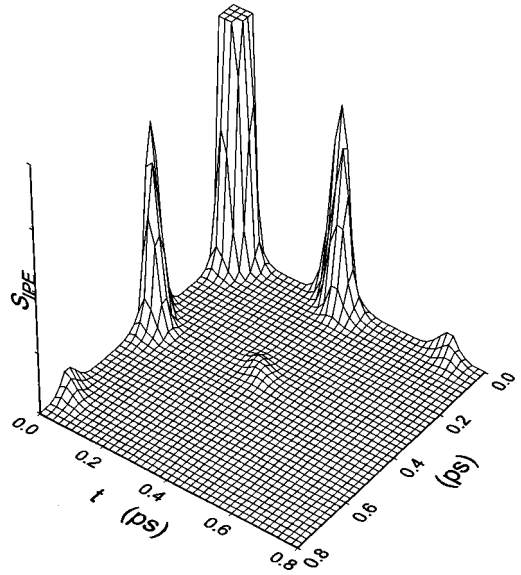

FIG. 10. The impulsive photon echo signal for (5) the excited-state quadratic perturbation case ($g_4'=0.08$). The free induction decay peak is approximately 20 times higher than is shown in the figure.

The first, second, and third pulses peak at time 0, T_1, and T_1+T_2, respectively, and we have included the phase ϕ in the probe pulse. Hereafter, we consider resonant pulses, i.e., Ω_j, Ω_j', etc. $\approx\omega_{eg}$ The probe signal with wave vector $\mathbf{k_f}=\mathbf{k_1}-\mathbf{k_1'}+\mathbf{k_2}-\mathbf{k_2'}+\mathbf{k_3}$ is then given by

$$S_5(\mathbf{k_f})=-2\ \mathrm{Im}\int_{-\infty}^{\infty}dtE_f(t-T_1-T_2-\delta)e^{i\phi+i\Omega_f t}\times P^{(5)}(\mathbf{k_f}=\mathbf{k_1}-\mathbf{k_1'}+\mathbf{k_2}-\mathbf{k_2'}+\mathbf{k_3},t), \tag{6.2}$$

where $P^{(5)}(\mathbf{k}_f,t)$ is the polarization in the direction $\mathbf{k}_f$. In the impulsive limit $\mu E_j(t)=\delta(t)$, the signal can be calculated from Eq. (4.16) by setting $t_1=t_3=0$, $t_2=T_1$, $t_4=T_2$, and $t_5=\delta$ as

$$S_5(\mathbf{k_f})=\mathrm{Re}\left[e^{i\phi}\sum_{\epsilon_2,\epsilon_4=\pm}R_{+\epsilon_1+\epsilon_4+}(0,T_1,0,T_2,\delta)\right], \tag{6.3}$$

where

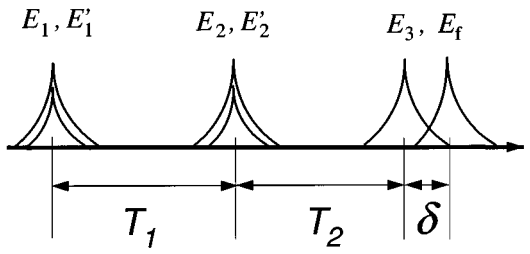

FIG. 11. Pulse configuration of the two-dimensional resonant spectroscopy. In this experiment, the time period δ must be small and fixed, since this then causes the signal to constitute a two-dimensional spectroscopy with two independent time periods T_1 and T_2 during which the wave packet evolves.

$$R_{\{\epsilon;5\}}(0,T_1,0,T_2,\delta)=\left[1-\frac{1}{\hbar}\int_0^{T_1}dt'V^2_{\{\epsilon;5\}}(t')-\frac{i}{\hbar}\int_{T_1}^{T_1+T_2}dt'V^4_{\{\epsilon;5\}}(t')-\frac{i}{\hbar}\int_{T_1+T_2}^{T_1+T_2+\delta}dt'V^5_{\{\epsilon;5\}}(t')-\frac{1}{\hbar}\int_0^{\beta\hbar}d\tau V^g_{\{\epsilon;5\}}(\tau)\right]\times\exp[Q_{\{\epsilon;5\}}(0,T_1,0,T_2,\delta)], \tag{6.4}$$

in which $\{\epsilon;N\}$ refers to the set $\{\epsilon_1,\epsilon_2,\ldots,\epsilon_N\}$, $V^j(\tau)$ are defined by Eqs. (3.15)–(3.17) with Eqs. (4.18)–(4.20), and

$$Q_{\{\epsilon;5\}}(0,T_1,0,T_2,\delta)=-g_{\epsilon_4}(\delta)-[g_{\epsilon_2}(T_1+T_2)-g_{\epsilon_2}(T_1+T_2+\delta)-g_-(T_1+T_2)+g_-(T_1+T_2+\delta)]-[g_{\epsilon_4}(T_2)-g_{\epsilon_4}(T_2+\delta)-g_{\epsilon_2}(T_2)+g_{\epsilon_2}(T_2+\delta)]. \tag{6.5}$$

It has been shown in the third-order experiments that the imaginary and real part of the polarization can be separately detected by choosing the phase ϕ.[44,45] In this paper, we present the real part signal (i.e., $\phi=0$), since this displayed larger effects of anharmonicity than the imaginary part in preliminary numerical calculations. For a fixed time δ, the above signal constitutes two-dimensional resonant spectroscopy (2DRS) with two independent time periods during which the wave packet evolves

$$S_{\mathrm{2DRS}}(T_1,T_2;\delta)=\mathrm{Re}\left[\sum_{\epsilon_2,\epsilon_4=\pm}R_{+\epsilon_2+\epsilon_4+}(0,T_1,0,T_2,\delta)\right]. \tag{6.6}$$

The essence of this experiment is the selection of the time δ. Equation (6.4) consists of the perturbation parts, inside the bigger set of the square braces, and the phase part, expressed in the exponential form. As seen from Eq. (6.5), the contributions of the phase part become small compared with the perturbation part, if δ is small ($\delta\ll 1/\omega_0$). Thus, for a fixed small δ, we can use this technique to detect the anharmonicity of the potentials. Note here that if we set $\delta=0$, then the signal will always be unity and we can not observe the difference of the potentials.

Figure 12 shows 2DRS for (1), the harmonic case, calculated from Eq. (6.6). To carry out numerical calculations, we set $\delta=0.01$ (ps). The signal consists of processes described by the different Liouville paths; (i) $gg\rightarrow ee\rightarrow ee\rightarrow eg$, (ii)$gg\rightarrow ee\rightarrow gg\rightarrow eg$, (iii) $gg\rightarrow gg\rightarrow ee\rightarrow eg$, and (iv) $gg\rightarrow gg\rightarrow gg\rightarrow eg$, denoted by the combination of sign parameters, $(\epsilon_2\epsilon_4\epsilon_5)=(+++),(+-+),(-++)$, and $(--+)$, respectively. Due to the assumption of the impulsive pulses, the shape of the wave packet does not change throughout the laser interaction. Thus, the contribution to the signal from process (iv) does not vary in time periods T_1 and T_2, since the wave packet is always in the ground-equilibrium state. The contribution from (iii) does not depend on T_1, since the wave packet is in the gg state in

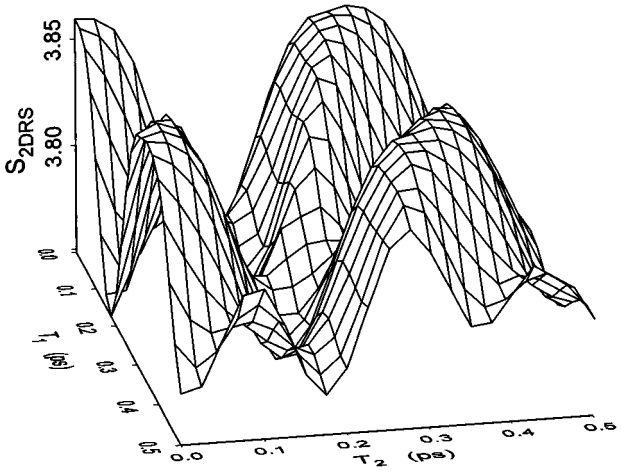

FIG. 12. The two-dimensional signal calculated from Eq. (6.6) for (1) the harmonic case ($g_j=0$ and $g_j'=0$).

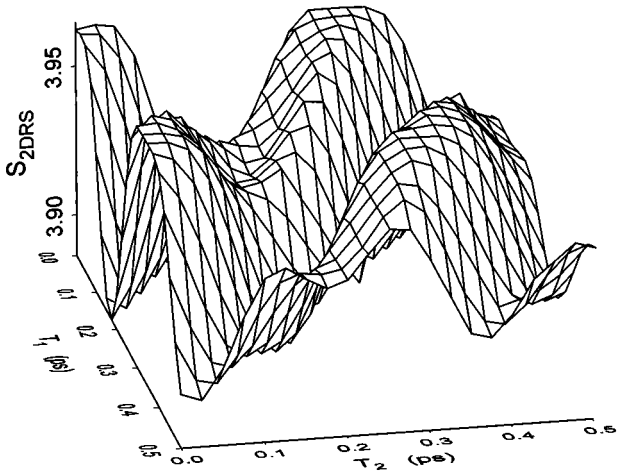

FIG. 13. The two-dimensional signal calculated from Eq. (6.6) for (2) the ground-state cubic perturbation case ($g_3=-0.08$).

this period, whereas the contribution from (ii) depends both on T_1 and T_2, since the wave packet created in the gg state through the ee state differs from the ground equilibrium state except for $T_1=0$. Finally, the contribution from (i) is a function of T_1+T_2, since both T_1 and T_2 periods describe the time propagation of the wave packet in the excited state. These four processes each show a different oscillating motion in the potentials, and thus we have a complicated structure of the signal as shown in Fig. 12.

We now consider the anharmonic cases. Figures 13–15 display 2DRS for (2), the ground-state cubic, (4) the excited-state cubic, and (5) the excited-state quadratic perturbation cases. We can observe clear differences between the harmonic and anharmonic cases in Figs. 13 and 15, the main difference being the enhancement of the signal along the lines $T_1+T_2=0.4$(ps) and $T_1+T_2=0.8$(ps). We have checked the origin of such enhancement for each of the Liouville paths and found that process (ii), $gg\rightarrow ee\rightarrow gg\rightarrow eg$ is the cause of such effects. While cases (2) and (5) show a clear difference from the harmonic one, case (4) is quite similar to it. Note that the signal for (3), the ground-state quadratic perturbation case, which is not shown here, also shows a profile similar to that of the harmonic one. As seen from Fig. 2, the phonon lines between $|g\rangle$ and $|e\rangle$ such as $1\rightarrow 0$, $0\rightarrow 0$, $0\rightarrow 1$, are lower than the harmonic case in these two cases. Therefore, an excitation in the ee state does not show a clear quantum beat at the resonant frequency and thus we could not observe a signal along lines $T_1+T_2=0.4$ and $T_1+T_2=0.8$, which originate from process (ii), $gg\rightarrow ee\rightarrow gg\rightarrow eg$. In such cases, 4DRS does not help to detect anharmonicity.

VII. CONCLUDING REMARKS

Although the present analysis has focused on the resonant spectroscopy of molecular systems, the model we have employed here has been widely used to describe such phenomena as elementary excitations, nonadiabatic transitions, and tunneling. The Nth order response functions presented in this paper may allow a characterization of the anharmonic system in the condensed phase, and can be applied to study such systems.

Although, in the present paper, we limit our study to a single mode system, generalization to a multimode system is straightforward. The corresponding response functions are given simply by the product of the single-mode response function as shown in Ref. 30. One often takes into account the inhomogeneity of the electronic transition energy by incorporating the overdamped oscillator mode.[42] Thus, by using the multimode system, the inhomogeneous broadening can be included in the present discussions.

A combination of experimental methods, such as linear absorption, pump–probe, and photon echo, may be necessary to elucidate the anharmonic contribution to the line. Fifth-order resonant spectroscopy, combined with such experiments, will allow the accurate decomposition of vibrational

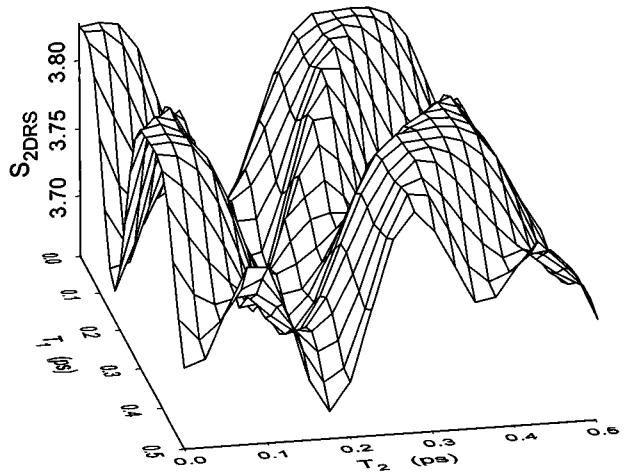

FIG. 14. The two-dimensional signal calculated from Eq. (6.6) for (4) the excited-state cubic perturbation case ($g_3'=-0.08$).

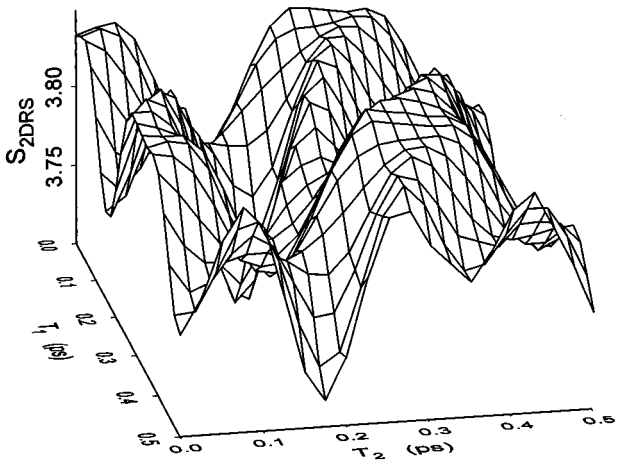

FIG. 15. The two-dimensional signal calculated from Eq. (6.6) for (5) the excited-state quadratic perturbation case ($g_4'=0.08$).

line shapes, that are convolutions of coherent and anharmonic oscillations. Although not discussed here, the expressions given in Sec. IV for the fifth-order polarization can also be used to study the fifth-order three pulses scattering (FOTS) proposed by Cho and Fleming, which was proposed to separate the homogeneous contribution of a vibrational spectrum from the inhomogeneity of the electronic transition energy. We have examined this direction of study using the expression we have obtained here to see effects of anharmonicity without the presence of the inhomogeneity, but, we could not observe a major change in the spectrum.

It is obvious that higher-order spectroscopy can contain many time intervals and these can be used to separate the targeting dynamical processes from the others; however, analysis of such signals becomes much more complex compared with the lower order ones. This is because, in addition to various physical parameters, one also needs to deal with various time configurations of lasers pulses in higher order optical processes, so simple theoretical expressions are essential to interpret the experimental studies. The response functions presented above provide a powerful means to explore such a direction of study.

ACKNOWLEDGMENTS

We thank K. Tominaga and K. Yoshihara for useful discussions. Financial support for this work was partially provided by Grand-in-Aid for Scientific Research from the Japan Ministry of Education, Science, Sports, and Culture.

[1] H. L. Fragnito, J. Y. Bigot, P. C. Becker, and C. V. Shank, Chem. Phys. Lett. **160**, 101 (1989).
[2] L. F. Fried and S. Mukamel, Adv. Chem. Phys. **84**, 435 (1993).
[3] K. Duppen, F. De Hann, E. T. J. Nibbering, and D. A. Wiersma, Phys. Rev. A **47**, 5120 (1993).
[4] J. T. Fourkas, H. Kawashima, and K. A. Nelson, J. Chem. Phys. **103**, 4393 (1995).
[5] D. Haarer and R. J. Silbey, Phys. Today **43**, 58 (1990).
[6] W. E. Moerner and T. Basche, Angew. Chem. **105**, 537 (1993).
[7] A. Laubereau and W. Kaiser, Rev. Mod. Phys. **50**, 607 (1978).
[8] D. P. Weitekamp, K. Duppen, and D. A. Wiersma, Phys. Rev. A **27**, 3089 (1983).
[9] S. Mukamel, *Principles of Nonlinear Optical Spectroscopy* (Oxford, New York, 1995).
[10] R. F. Loring and S. Mukamel, J. Chem. Phys. **83**, 2116 (1985).
[11] D. Vanden Bout, L. J. Muller, and M. Berg, Phys. Rev. Lett. **67**, 3700 (1991); D. Vanden Bout, L. Muller, J. Freitas, and M. Berg, in *Ultrafast Phenomena IX*, edited by G. Mourou, A. Zewail, P. F. Barbara, and W. H. Knox (Springer, Berlin, 1994); L. J. Muller, D. Vanden Bout, and M. Berg, J. Chem. Phys. **99**, 810 (1993); D. V. Bout, J. E. Freitas, and M. Berg, Chem. Phys. Lett. **299**, 87 (1994).
[12] M. D. Fayer, Annu. Rev. Phys. Chem. **33**, 63 (1982); J. T. Fourkas and M. D. Fayer, Acc. Chem. Res. **25**, 227 (1992).
[13] M. Müller, K. Wynne, and J. D. W. Van Voorst, Chem. Phys. **125**, 211, 255 (1988).
[14] R. Inaba, K. Tominaga, M. Tasumi, K. A. Nelson, and K. Yoshihara, Chem. Phys. Lett. **211**, 183 (1993); K. Yoshihara, R. Inaba, H. Okamoto, M. Tasumi, K. Tominaga, and K. A. Nelson, in *Femtosecond Reaction Dynamics*, edited by D. R. Wiersma (North–Holland, Amsterdam, 1994); K. Tominaga, R. Inaba, T. J. Kang, Y. Naitoh, K. A. Nelson, M. Tasumi, and K. Yoshihara, in *Proceedings of the XIV International Conference on Raman Spectroscopy* (Wiley, New York, 1994); K. Tominaga, Y. Naitoh, T. J. Kang, and K. Yoshihara, in *Ultrafast Phenomena IX*, edited by G. Mourou, A. Zewail, P. F. Barbara, and W. H. Knox (Springer, Berlin, 1994).
[15] D. Zimdars, A. Tokmakoff, S. Chen, S. R. Greenfield, and M. D. Fayer, Phys. Rev. Lett. **70**, 2718 (1993); A. Tokmakoff, D. Zimdars, B. Sauter, R. S. Francis, A. S. Kowk, and M. D. Fayer, J. Chem. Phys. **101**, 1741 (1994).
[16] Y. Tanimura and S. Mukamel, J. Chem. Phys. **99**, 9496 (1993).
[17] S. Palese, J. T. Buontempo, L. Schilling, W. T. Lotshaw, Y. Tanimura, S. Mukamel, and R. J. D. Miller, J. Phys. Chem. **98**, 12 466 (1994).
[18] K. Tominaga and K. Yoshihara, Phys. Rev. Lett. **74**, 3061 (1995); K. Tominaga, G. P. Keogh, Y. Naitoh, and K. Yoshihara, J. Raman Spectrosc. **26**, 495 (1995); K. Tominaga and K. Yoshihara, J. Chem. Phys. **104**, 1159 (1996); **104**, 4422 (1996).
[19] T. Steffen and K. Duppen, Phys. Rev. Lett. **76**, 1224 (1996); T. Steffen, J. T. Fourkas, and K. Duppen, J. Chem. Phys. **105**, 7364 (1996); T. Steffen and K. Duppen, J. Chem. Phys. (in press).
[20] A. Tokmakoff, J. Chem. Phys. **105**, 13 (1996); A. Tokmakolf and G. R. Fleming, J. Chem. Phys. (in press).
[21] J. A. Leegwater and S. Mukamel, J. Chem. Phys. **102**, 2365 (1995).
[22] K. Okumura and Y. Tanimura, J. Chem. Phys. **105**, 7294 (1996); (submitted).
[23] M. Cho and G. R. Fleming, J. Phys. Chem. **98**, 3478 (1994).
[24] T. Joo, Y. Jia, and G. R. Fleming, J. Chem. Phys. **102**, 4063 (1995).
[25] V. May, O. Kühn, and M. Schreiber, J. Phys. Chem. **97**, 12 591 (1993); O. Kühn, V. May, and M. Schreiber, J. Chem. Phys. **101**, 10 404 (1994).
[26] Y. Tanimura and S. Mukamel, J. Chem. Phys. **101**, 3049 (1994).
[27] N. Bloembergen, *Nonlinear Optics* (Benjamin, Massachusetts, 1965).
[28] S. Chakravarty and A. J. Leggett, Phys. Rev. Lett. **52**, 5(1984); A. J. Leggett, S. Chakravarty, A. T. Dorsey, M. P. A. Fisher, A. Garg, and W. Zwerger, Rev. Mod. Phys. **59**, 1 (1987); **67**, 725 (E) (1995).
[29] A. Garg, J. N. Onuchic, and V. Ambegaokar, J. Chem. Phys. **83**, 4491 (1985).
[30] Y. Tanimura and S. Mukamel, Phys. Rev. E **47**, 118 (1993); J. Opt. Soc. Am. B **10**, 2263 (1993); in *Ultrafast Spectroscopy in Chemical Systems*, edited by J. D. Simon (Kluwer, Dordrecht, 1994), p. 327.
[31] K. Okumura and Y. Tanimura, Phys. Rev. E **53**, 214 (1996).
[32] R. Kubo and Y. Toyozawa, Prog. Theor. Phys. **13**, 160 (1955).
[33] *Relaxation of Elementary Excitations*, edited by R. Kubo and E. Hanamura (Springer, Berlin, 1980).
[34] Y. R. Shen, *The Principles of Nonlinear Optics* (Wiley, New York, 1984).
[35] Y. J. Yan and S. Mukamel, J. Chem. Phys. **94**, 997 (1991); Phys. Rev. A **41**, 6485 (1990).
[36] R. W. Hellwarth, Prog. Quantum Electron. **5**, 1 (1977).
[37] R. A. Marcus, J. Chem. Phys. **24**, 966, 979 (1956); Ann. Phys. Chem. **15**, 155 (1964).
[38] P. G. Wolynes, J. Chem. Phys. **86**, 1957 (1987); **87** 6559 (1987); J. N. Onuchic and P. G. Wolynes, J. Phys. Chem. **92**, 6495 (1988).

[39] M. Sparpaglione and S. Mukamel, J. Chem. Phys. **88**, 3263, 4300 (1988).
[40] D. Devault, *Quantum-Mechanical Tunneling in Biological Systems*, 2nd ed. (Cambridge University Press, New York, 1984).
[41] P. Hänggi, P. Talkner, and M. Borkovec, Rev. Mod. Phys. **62**, 251 (1990).
[42] H. Grabert, P. Schramm, and G-L Ingold, Phys. Rep. **168**, 115 (1988).
[43] W. B. Bosma, Y. J. Yan, and S. Mukamel, Phys. Rev. A **42**, 6920 (1990).
[44] W. P. de Boeij, M. S. Pshenichnikov, and D. A. Wiersma, Chem. Phys. Lett. **238**, 1 (1995).
[45] M. S. Pshenichnikov, W. P. de Boeij, and D. A. Wiersma, Phys. Rev. Lett. **76**, 4701 (1996).